# INVESTIGATION OF THE EFFECT OF WATER REDUCERS ON THE SLAG-BASED ALKALI-ACTIVATED MATERIAL

**Noora Khasro SALEH**

**2022**
**MASTER THESIS**
**CIVIL ENGINEERING**

**Thesis Advisor**
**Assoc. Prof. Dr. İlker TEKİN**

# INVESTIGATION OF THE EFFECT OF WATER REDUCERS ON THE SLAG-BASED ALKALI-ACTIVATED MATERIAL

**Noora Khasro SALEH**

**T.C.**
**Karabuk University**
**Institute of Graduate Programs**
**Department of Civil Engineering**
**Prepared as**
**Master Thesis**

**Thesis Advisor**
**Assoc. Prof. Dr. İlker TEKİN**

**KARABUK**
**Septemter2022**

I certify that in my opinion, the thesis submitted by Noora Khasro Saleh titled "INVESTIGATION OF THE EFFECT OF WATER REDUCERS ON THE SLAG-BASED ALKALI-ACTIVATED MATERIAL" is fully adequate in scope and quality as a thesis for the degree of Master of Science.

Assoc. Prof. Dr. İlker TEKİN .....
Thesis Advisor, Department of Civil Engineering

This thesis is accepted by the examining committee with a unanimous vote in the Department of Civil Engineering as a Master of Science thesis. Sep 23, 2022

| Examining Committee Members (Institutions) | Signature |
|---|---|
| Chairman : Prof. Dr. H. Yılmaz ARUNTAŞ (GU) | ..... |
| Member : Assoc. Prof. Dr. İlker TEKİN (KBU) | ..... |
| Member : Assist. Prof. Dr. Mustafa DAYI (DU) | ..... |

The degree of Master of Science by the thesis submitted is approved by the Administrative Board of the Institute of Graduate Programs, Karabuk University.

Prof. Dr. Hasan SOLMAZ .....
Director of the Institute of Graduate Programs

*"I declare that all the information within this thesis has been gathered and presented in accordance with academic regulations and ethical principles and I have according to the requirements of these regulations and principles cited all those which do not originate in this work as well."*

Noora Khasro SALEH

## ABSTRACT

**M. Sc. Thesis**

**INVESTIGATION OF THE EFFECT OF WATER REDUCERS ON THE SLAG-BASED ALKALI-ACTIVATED MATERIAL**

**Noora Khasro SALEH**

**Karabuk University**
**Institute of Graduate Programs**
**Department of Civil Engineering**

**Thesis Advisor:**
**Assoc. Prof. Dr. İlker TEKİN**
**September 2022, 78 pages**

In this study, the main objective is to determine the effects of superplasticizers on the fresh and mechanical properties of geopolymer pastes. In this scope, Energy Transferring System ash and Ground Granulated Blast Furnace Slag (GGBFS) from the Kardemir Iron&Steel industry were used as alumina silicate sources to produce alkaline activated geopolymer pastes (AAGP), and sodium silicate ($Na_2SiO_3$) with/without 10 M concentrated sodium hydroxide (NaOH) were used as activators. Two types of water reducers (Sulfonated Melamine Formaldehyde and polycarboxylate ether-based SPs) were used to investigate SP effects. Moreover, sintering ash from the Kardemir Iron&Steel industry was used as an additional activator with different ratios to improve the workability and mechanical and physical properties. Two different experimental studies were conducted to determine fresh state properties and hardened state properties, respectively. Marsh funnel, flow table, and setting time tests were carried out on fresh-state AAGP, and also

compressive strength and water absorption tests on the 2nd, 28th, and 90th ages were carried out on hardened-state AAGPs. The results of this study showed maximum 90 days compressive and flexural strengths for the first study were 18 MPa and 7.5 MPa respectively. However, the ideal value of marsh funnel time, flow spreading diameter, and setting time were 3.3 seconds, 225 minutes, and 33 cm for mixtures N-SPK2, S0, and N-S0, respectively. The results of the second study maximum 28 days compressive strengths for 20% and 10% of NaOH were 41.75 MPa and 36.95 MPa respectively, and the water absorption for AAGP batches ranged between 13.17 – 19.97 percent.

**Key Words :** Alkali-Activated geopolymer paste, Superplasticizer, Sintering ash, Sulfonated Melamine Formaldehyde, Polycarboxylate ether, ETM ash, Ground granulated blast furnace slag, Marsh funnel.

**Science Code :** 91127

# ÖZET

**Yüksek Lisans Tezi**

## SU AZALTICILARIN CÜRÜF BAZLI ALKALİ AKTİF MALZEME ÜZERİNE ETKİSİNİN İNCELENMESİ

**Noora Khasro SALEH**

**Karabük Üniversitesi**
**Lisansüstü Eğitim Enstitüsü**
**İnşaat Mühendisliği Anabilim Dalı**

**Tez Danışmanı:**
**Doç. Dr. İlker TEKİN**
**Eylül 2022, 78 sayfa**

Bu çalışmanın temel amacı süper akışkanlaştırıcıların jeopolimer hamurların taze ve mekanik özellikleri üzerindeki etkilerinin belirlemektir. Bu kapsamda, Kardemir Demir-Çelik sektöründen Enerji Aktarım Sistemi külü ve Öğütülmüş Granül Yüksek Fırın Cürufu (GGBFS) alümina silikat kaynağı olarak ve 10 M derişimli sodyum hidroksitli/siz sodyum silikat ($Na_2SiO_3$) çözeltisi aktivatör olarak alkali aktive edilmiş geopolimer hamur (AAGP) üretiminde kullanılmıştır. Süperakışkanlaştırıcı (SP) etkilerini araştırmak için Sülfonatlı Melamin Formaldehit ve polikarboksilat eter bazlı iki tip SP su azaltıcı olarak kullanıldı. Ayrıca Kardemir Demir-Çelik endüstrisinden gelen sinterleme külü, işlenebilirliği, mekanik ve fiziksel özellikleri iyileştirmek için farklı hacim oranlarında ilave aktivatör olarak kullanıldı. Sırasıyla taze hal özelliklerini ve sertleştirilmiş hal özelliklerini belirlemek için iki farklı deneysel çalışma gerçekleştirilmiştir. Taze durumdaki AAGP'de Marsh hunisi, akış tablosu ve priz süresi testleri ve sertleştirilmiş durumdaki AAGP'lerde 2, 28 ve 90

gün yaşlarında basınç dayanımı ve su emme testleri gerçekleştirilmiştir. Bu çalışmanın sonuçları, ilk çalışma için maksimum 90 günlük basınç ve eğilme dayanımlarının sırasıyla 18 MPa ve 7,5 MPa olduğunu göstermiştir. Ancak, N-SPK2, S0 ve N-S0 karışımları için bataklık hunisi süresi, akış yayılma çapı ve priz süresinin ideal değeri 3,3 saniye, 225 dakika ve 33 cm'dir. sırasıyla. İkinci çalışmanın sonuçları, %20 ve %10 NaOH için en fazla 28 günlük basınç dayanımları sırasıyla 41,75 MPa ve 36,95 MPa idi, AAGP partileri için su emme yüzde 13,17 – 19,97 arasında değişiyordu.

**Anahtar Kelimeler :** Alkali Aktive edilmiş jeopolimer hamur, süper akışkanlaştırıcı, Sinter külü, Melamin Formaldehit, Polikarboksilat eter, ETM külü, Öğütülmüş yüksek fırın cürufu, Marsh Funnel.

**Bilim Kodu** **:** 91127

## ACKNOWLEDGMENT

I owe thanks and praise first and foremost to Allah the Almighty for this success and facilitation as I bow to my beloved parents. My dear father gave me the most precious things to make me a man of honor. My beloved mother is good at engineering my heart with her prayers. To my family in which I grow up and its extension that gives me pride and honor. I owe a special thanks to my thesis supervisor, Assoc. Prof. Dr. İlker TEKİN spared no effort in providing unlimited advice and guidance until the completion of this thesis to the fullest image.

I also extend my thanks and gratitude to the University of Karabuk, including the wonderful professors, doctors, and colleagues who accompanied us throughout our academic journey.

I dedicate this thesis to my beloved country, Iraq. And to the beautiful Turkey, which embraced this scientific experiment and contributed to providing all possibilities to graduate in this distinguished way.

**CONTENTS**

**Page**

**Page**

**Page**

## LIST OF FIGURES

**Page**

**Page**

## LIST OF TABLES

**Page**

## SYMBOLS AND ABBREVIATIONS INDEX

### SYMBOLS

| | |
|---|---|
| % | : Percent Sign |
| m | : Meter |
| cm | : Centimeter |
| mm | : Millimeter |
| μm | : Micrometer |
| Kg | : Kilogram |
| $^{o}$C | : Degrees Celsius |

### ABBREVIATIONS

| | |
|---|---|
| AAM | : Alkali Activated Material |
| AAFA | : Alkali-Activated Fly Ash |
| AAS | : Alkali Activated Slag |
| AAC | : Alkali-Activated Concrete |
| OPC | : Ordinary Portland Cement |
| FA | : Fly Ash |
| GGBS | : Ground Granulated Blast-Furnace Slag |
| C-S-H | : Calcium Silicate Hydrate |
| C-A-S-H | : Calcium aluminate silicate hydrate |
| N-A-S-H | : Sodium-Aluminosilicate-Hydrate |

# PART 1

## INTRODUCTION

For its extraordinary properties like low costs, high strength, and excellent durability, concrete is second only to water in terms of global usage, and it plays a significant role in the construction industry. Ordinary Portland Cement (OPC) is a key ingredient in the producing of concrete. However, in the production of cement, a significant amount of Carbon Dioxide ($CO_2$) released into the atmosphere, which has negative effects on the natural environment. Producing one ton of OPC results in the release of one ton of $CO_2$ [1]. This is considered to be a massive one, since the approximate production of concrete has been estimated to be 1 $m^3$ per person [2]. Cement production requires huge amounts of fuel, leading to massive amounts of carbon dioxide emissions and consequently it causes global warming problems. There has been a steady rise in cement production since the turn of the millennium, by a factor of about 78%. This has resulted in a rise of 5-8% in anthropogenic $CO_2$ emissions [3]. Moreover, cement production consumes about 12–15% of the world's annual industrial energy resources [4]. Scientists have been trying to find an alternative to OPC. According to the scientist have been studying on alternative binders, alkali-activated materials and geopolymers can be preferred instead of OPC because of their superior mechanical and physical properties [5,6].

The research conducted by Purdon in the 1940s laid the groundwork for the creation of alkali-activated materials (AAMs) [7]. Purdon used blast furnace slag with the addition of a sodium hydroxide solution to prepare AAMs. However, the global recognition of this material was inaugurated to develop in the the1950s in Eastern Europe with the work generated by Glukhovsky and his team. When a solid aluminosilicate source is activated with an alkaline solution, a geopolymerization reaction takes place, which results in AAMs. Solid aluminosilicate sources can be obtained from a variety of places, the most common of which are blast furnace slag,

metakaolin, and fly ash (FA) [8,9]. Several activators, such as sodium sulfate ($Na_2SO_4$), sodium carbonate ($Na_2CO_3$), sodium hydroxide (NaOH), potassium hydroxide (KOH), sodium silicate ($Na_2SiO_3$), potassium silicate ($K_2SiO_3$), and calcium hydroxide ($Ca(OH)_2$), can be used singly or in combination to bring those sources into use [10]. The AAMs are made from a different set of hydration products of the geopolymerization reactions than those used to make OPC. Sodium-aluminosilicate-hydrate (N-A-S-H) and calcium-aluminosilicate-hydrates (C-A-S-H) are the two most abundant byproducts of the geopolymerization reaction. However, Calcium-silicate-hydrate (C–S–H) is the most common hydrated product in OPC systems [11].

One of the more promising materials, AAMs boast impressive mechanical and physical properties. For example, Ümit Yurt (2020) [12] conducted research into the use of alkali-activated slags to create cementless composites with high performance. The samples were tested for Dynamic Modulus of Elasticity, compressive strength, splitting tensile strength, and abrasion resistance. Based on the findings, they infer that using 100% slag enabled AAM production. As for the cement-free concretes, they were able to achieve a compressive strength of 82.32 MPa by incorporating slag into the mix. Activation was formed in Alkali-Activated Concrete (AAC) samples using 8 M, 10 M, and 12 M aqueous solutions of sodium hydroxide and sodium silicate. Abhilash et al. (2017) [13] conducted a study to compare OPC concrete and geopolymer concrete's ability to withstand acidic conditions. They measure the samples' resistance using compression strength and weight change. Contrast to the OPC concrete, geopolymer concrete proved to be extremely resistant to both sulphuric and hydrochloric acid. Researchers have compared the material's mechanical and physical properties to those of OPC. Alkali-activated slag (AAS) has been shown to have superior properties to regular concrete in many different research areas [14,15]. Thus, this material can be suitable to be used as a replacement for conventional concrete soon.

The addition of superplasticizer (SP) admixtures changed the rheology of cement paste, as shown by numerous studies. The findings suggest that the incorporation of fly ash into cement requires the addition of water reducers to ensure that the resulting

cement paste is consistently workable without the addition of any additional water. The amount of SP is greatly influenced by the amount of OPC that is replaced with ashes, and considerably less so by the type of addition [16].

Adding 0.22 wt% of a polycarboxylate ether cement admixture will raise the cement's class from commercial CEM II/A-V 42.5R (Blaine surface of 460 $m^2$/kg) to CEM II/A-V 52.5N. Fly ash cement with added SPs exhibits better mechanical properties than the control sample, though the increase in compressive strength value is not as dramatic as in the case of polycarboxylate ether (PCE). Cement CEM II/A-V 42.5R is formulated by mixing sulfonated melamine-formaldehyde (SMF) condensate (0.57 wt%) with sulfonated naphthalene-formaldehyde (SNF) condensate (0.33 wt%) [17].

The compressive strength of fly ash cement is enhanced by adding SP after 28 days, but only if the recommendation of an admixture amount of 1.0 wt% is used. Results for mixtures in other studies show only a slight variation, which may be attributable to the fact that the concentration of each SP was much lower than 1.0%. If the current admixture dosage levels are below the optimal dosage, only an increase in admixture dosage may help to improve the compressive strength of cement mortar [18].

Tkaczewska [19] explain how various SPs affect the properties of the blended fly ash cement. Both polycarboxylate ether (PCE) and polycarboxylate (PC) from the next generation of SPs reduce water content by 47% and 42%, respectively, compared to other SPs like sulfonated naphthalene formaldehyde (SNF) and sulfonated melamine formaldehyde (SMF). Mechanical properties of the OPC mortars are enhanced when a blended mix containing fly ash.

With the addition of polycarboxylate ethylene-based SP, mixes with increasing amounts of fly ash exhibit greater compressive strength. When fly ash is combined with a SP based on PCE, the pore size decreases, resulting in a slower water absorption rate [20].

As conventional concrete, AAMs have some undesirable properties sometime, or some properties need to be improved. Thus, in the fresh mixes, admixtures could be used to close these gaps. Like conventional concrete, Patel and Shah (2018) [16] made an effort to achieve 30 MPa strength with Rice Husk Ash as an admixture in a study of self-compacted geopolymer concrete. We found that a maximum compressive strength of 42.60 MPa could be achieved with this admixture. Shahrajabian and Behfarnia (2018) [21] performed a study on the behavior of alkali-activated slag concretes with nano-silica, nano-alumina, and nano-clay admixtures when exposed to freeze-thaw cycles. The results demonstrated that the admixtures improved the mixes' properties, with nano-silica and nano-clay demonstrating superior results in terms of strength and durability properties to those of using nano alumina in the alkali-activated slag concrete mixes. Karthik et al. (2017) [22] materials such as fly ash and slag to create geopolymer concretes. They used 30 degrees Celsius (room temperature) as the curing temperature for the concrete samples and two different molarities (4 mol and 8 mol) to achieve different results. Natural sugars and the bio-additive Terminalia Chebula were used to create the geopolymer. Based on the data, they determined that at 28 days, the compressive strength reached a maximum of 37.24 MPa. Based on their research, they concluded that the addition of bio-additives to concrete improved its workability and mechanical properties.

The workability of AAFS declined as slag concentration and SH molarity increased, along with a decline in the AL/B ratio. Slag content appeared to have a greater impact at higher SH molarities and higher AL/B ratios. In comparison to specimens with lower slag concentration, specimens with higher SH molarity at higher slag replacement levels showed a more noticeable loss of workability [23]. The testing results showed that the type of activator and the SP strongly influence how well a fly ash-based geopolymer works and how strong it is [24].

Many other properties about conventional concrete could be developed by using different types of admixtures. Those admixtures could be used for AAMs; however, it may give another result due to the lack of studies on AAMs with admixtures. This study will focus on examining the properties of the AAMs using water reducer

admixtures in raw statement (in powder condition). In this experimental study, different water-reduction percentages in the mixes were used to prepare slag-based AAM. Samples were tested at 2, 28, and 90 days into production to assess mechanical and physical properties like flexural strength, compressive strength as well as workability features.

## 1.1. THESIS SCOPE, AIM AND OBJECTIVES

### 1.1.1. Subject and Scope

The purpose of this research is to create alkali-activated materials from ground granulated blast-furnace slag by combining various amounts of water reducers with the mixes. Currently, there are very few studies examining alkali-activated materials or their properties with SPs in raw state additives. This study is going to examine the mechanical behavior effect using water reducers.

### 1.1.2. Aim and Objective

This thesis aims to make Slag Based Alkali-Activated Material and investigate the effect on the Mechanical properties when Water Reducers are added to the mixes to improve the workability that results in high compressive strength.

### 1.1.3. Objective

- To obtain a higher compressive and flexural strength by using water reducers.
- To increase the water resistance of hardened mixes by using water reducers.
- To produce an economical alkali-activated material mix by using water reducers.

## 1.2. THESIS ARRANGEMENT

As for the rest of the thesis, it is set up as follows:

**Part 2:** Background of the Alkali activated materials and most used additives and admixtures worldwide.

**Part 3:** Illustrates the approach done to produce the pastes and the test applied in the fresh and hardened pastes.

**Part 4:** Illustrates and discusses the test results.

**Part 5:** The conclusion part and the summary of this study are based on the results.

# PART 2

# LITERATURE REVIEW

## 2.1. CHALLENGES FACING THE CEMENT INDUSTRY

Concrete is widely acknowledged to be one of the most widely utilized materials of the world. Because of its low cost and high-quality mechanical and physical properties, this material is increasingly being used in the building industry. However, one of the main components of this material is Portland Cement (PC). However, PC is one of the most pollutant materials to the environment. Almost 7% of the world's annual greenhouse gas emissions have been released into the atmosphere, as a result of the production of PC [25]. One ton of cement production causes approximately one ton of carbon dioxide into the atmosphere and the most harmful thing is to be increasing of PC production about 3% annually [1, 26]. Thus, the total demand for PC would increase by almost 200% from 2010 to 2050 [22]. Alkali-activated materials (AAM) can be the most promising alternative binders currently because they have environmental performance and give satisfying mechanical and physical properties [6,28].

## 2.2. ALKALI ACTIVATED MATERIALS

### 2.2.1. Historical Developments of Alkali Activated Cement and Concretes

Studies on the AAM have been started by using alkali in a cementitious material as a component by Kuhl in 1930 [29]. Purdon analyzed the setting behavior of various pre-mixes of ground blast furnace slag activated by a solution of caustic potassium. Moreover, extensive research on types of cement mainly consisting of slag and caustic alkalis activated by an alkaline salt was performed. [30]. AAMs became more popular thanks to Glukhovsky’s studies in 1957 [31]. He was the first to recognize

that aluminosilicate and alkali metal solutions could be used in cement pastes, and he coined the term "soil cement" to match the term "soil silicates" for concrete [32]. At that time, the binders were divided into two primary groups the alkaline binding system ($Me_2O$-$Me_2O_3$-$SiO_2$-$H_2O$) and the earth alkali binding system ($Me_2O$–MeO–$Me_2O_3$–$SiO_2$–$H_2O$) [33].

Davidovits played a key role in developing this material in 1979. Davidovits developed this material and patented a new binding structure that has some similarities to the system of alkaline binding. According to Davidovits, the main substances in the AAM are aluminosilicate components as the byproducts of sintering kaolinite and limestone or dolomite. He derived a new term called "geopolymer" for his patented material to highlight the similarities between this binder and the earth mineral found in stones like marble and granite [34]. Nowadays, this term is commonly used to refer to AAM systems. Moreover, in his opinion, these materials helped the early ancient Egyptians and Romans to build their constructions as well [35].

In 1994 Krivenko argued that there is a distinction in the roles of alkali elements in terms of acceleration of setting and structure-forming in a system [35,36]. Afterward, extensive research on alkali-activated binders has been conducted on the activation of fly ash and Alkali-slag cement [37]. This material started to grow quickly after increasing the studies on it and many applications for this material have been adopted [38]. The most well-known names for this material are Alkali-activated cement, Geopolymers, and Geocements [35].

### 2.2.2. Types and Mechanisms of AAM

AAM is a type of material that is produced mainly by a resource of aluminosilicate precursor that should be activated by an alkaline solution. After the activation, the material starts to get strength over time by creating bonding structures similar to cement [30]. This material can be produced by using most aluminosilicate sources; but using various types of aluminosilicates will lead to different reaction mechanisms. Each reaction mechanisms are a geopolymerization process. One of the

mechanisms is based on the alkaline activation of aluminosilicate-based binders such as the activation of F-type fly ash and Metakaolin [40], and the other one is based on the alkaline activation of the calcium-bearing system such as the activation of type C fly ash and slag [41]. Hence, ground granulated blast furnace slag (GGBFS), rice husk ash (RHA), fly ash (FA), and metakaolin are only some of the commonly utilized materials to produce AAM. In general, the terms used to describe for this material are geopolymers and alkali-activated materials. Both words refer to materials that are formed from aluminosilicate precursors, but the precursors used to form each type of material have a distinct $Al^{3+}$ and $Ca^{2+}$ concentration. Cementation materials are depicted in Figure 2.1. [42].

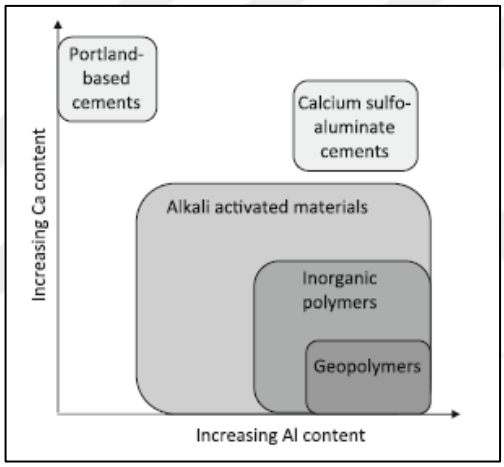


Figure 2.1.The types of cementations materials [42].

### 2.2.2.1. Geopolymerization Process

Since, in this reaction, the alkali solution causes the dissolving of cations in activation duration, the geopolymerization process is thought to generate heat like an exothermic polycondensation reaction [42]. Equations 2.1 and 2.2 shows the reaction mechanism that results in the formation of a polysialates geopolymer [43]. Equation 2.3 describes the end product after the geopolymerization reaction process is complete. This equation also includes the cation that was used to initiate the reaction, the degree of polycondensation, and the polysialate, polysialate-siloxo, and polysialate-disiloxo structures, with z = 1, 2, and 3, respectively [46].

$$(Al_2Si_2O_7)_n + nH_2O \xrightarrow{MOH} n(OH)_3 - Si - Al - (OH)_3 \quad (2.1)$$

$$n(OH)_3 - Si - O - Al - (OH)_3 \xrightarrow{MOH} M\left(-Si(O) - O - Al^{(-)}(O) - O\right)_n + nH_2O \quad (2.2)$$

$$M_n\{-(SiO_2)z-(AlO_2)\}n + H_2O \text{ [45]} \quad (2.3)$$

As can be seen from the equations, to generate either the polysialate-siloxo or polysialates-disiloxo structures of AAM, in addition to the extra amounts of amorphous silica, M defines the cation utilized to activate the reaction, which is commonly provided KOH or NaOH. To understand the distinction between the two reactions, the polysialate-siloxo formation reaction is given in Figure 2.2 [44].

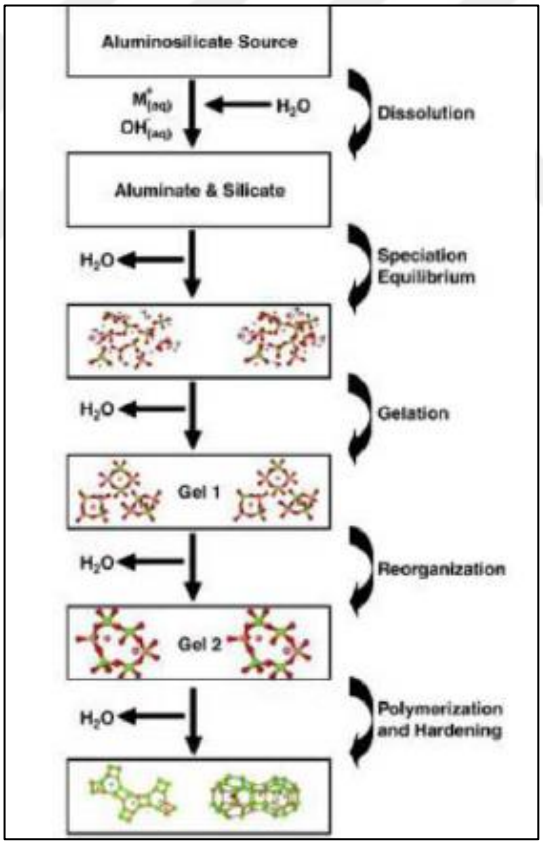


Figure 2.2. Geopolymerization process [45].

The materials rich in silicon (Si) and aluminum (Al) are used to produce AAM. Alkali-activated cement has three distinct versions: 1) Activation of materials comprising primarily aluminum and silicon, along with low calcium concentrations.

In this model, metakaolin or Class F fly ash is used for the alkali activation process. The curing condition plays a key role in this type of reaction. Heat curing gives more efficiency results, especially between 60 and 200 ºC. This model creates a zeolite precursor in the form of a three-dimensional alkaline inorganic polymer, namely an alkaline aluminosilicate gel [46,47]. 2) Slag and other calcium- and silicon-rich materials are activated. The primary byproduct of this type of reaction is calcium silicate hydrate (C-S-H) gel-like [48]. 3) The result of this type is a blend of the previous two models [49].

**Alkaline Activation of Aluminosilicate-Based Binders**

Usually, “polysialate" term is used for the molecular structures of geopolymers. The term is derived from "silico aluminate". As can be seen in Figure 2.3, the network is made up of $SiO_4$ and $AlO_4$ tetrahedrons held together by oxygen atoms [50]. The negative charge of the $Al^{+4}$ tetrahedron in IV-fold coordination necessitates the presence of positive ions to counteract it. Positive ions ($Na^+$, $K^+$) must compensate for the negative charge, so alkalis are utilized as the activating agents. Several =Si-O-Si= bonds connecting a specific Si atom to its immediate neighbors [50].

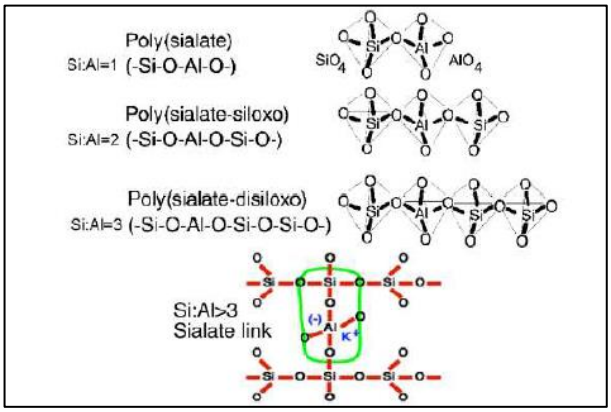


Figure 2.3. SiO4 and AlO4 network [50].

Fly ash can be an example of a source of aluminosilicate reach materials [51]. When fly ash is treated with alkali, the glassy phase's covalent bonds (Si-O-Si and Al-O-Al) are broken and released into the solution, resulting in an exothermic process [51,52]. Afterward, a chain reaction begins with the fly ash particles becoming unstable [52].

The dissolved substances begin to gather for a period, and during this time, the rate of releasing heat is low, and the reaction products start to be generated inside and outside of the sphere surface. This process remains until entirely or almost wholly fly ash particles are transformed into new reaction products. This mechanism is illustrated in Figure 2.4. The precipitations of the reaction products happen along with the previous products. On the other hand, the activator solution flows thorough the bigger sphere's interior, where it mixes with the reaction product and forms a dense matrix (Figure 2.4b). While this process is happening, some smaller fly ash particles are covered with the reaction products, leading to blocking the alkali activator solution to reach the Fly ash particle shell and inhibit the reaction of covered particles (Figure 2.4c). The final product may include several morphology types such as unreacted fly ash particles, alkaline solution-attacked particles that lost their spherical shape, and reaction products (Figure 2.4d) [52].

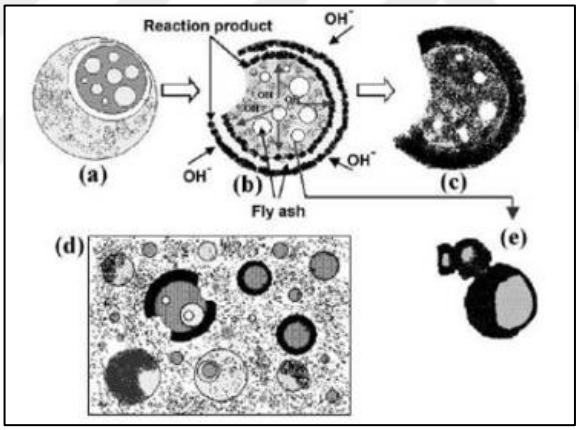


Figure 2.4. Alkali activation of fly ash mechanism [52].

**Alkaline Activation of Calcium-Bearing System**

Aluminosilicates-based binders and calcium-bearing compounds react in different ways [53]. The alkali activation of these materials depends critically on the sort of calcium-bearing basis of the starting substance. The reaction duration contains several stages. The first stage in this reaction starts with the destruction of the raw material. The reaction process of alkali-activated slag starts with the dissolve of a glassy Ca-Si particle shown in Figure 2.5. In Step A, during the reaction, the ion exchange of $H^+$ with $Ca^{2+}$ and $Na^+$ among the slag particles' surface begins in an

alkali solution. In Step B, the Al-O-Si bonds are hydrolyzed. In Step C, the entire glassy phase is disrupted as the depolymerized glass network begins to break down. This stage is characterized by the breakdown of most activated materials and primarily slag, in particular Ca-O and T-O bonds. The final step involves the beginning of the Si and Al release and the appearance of the Si-Al layer close to the surface of the activated particle, followed by the generation of the results of the reaction [53].

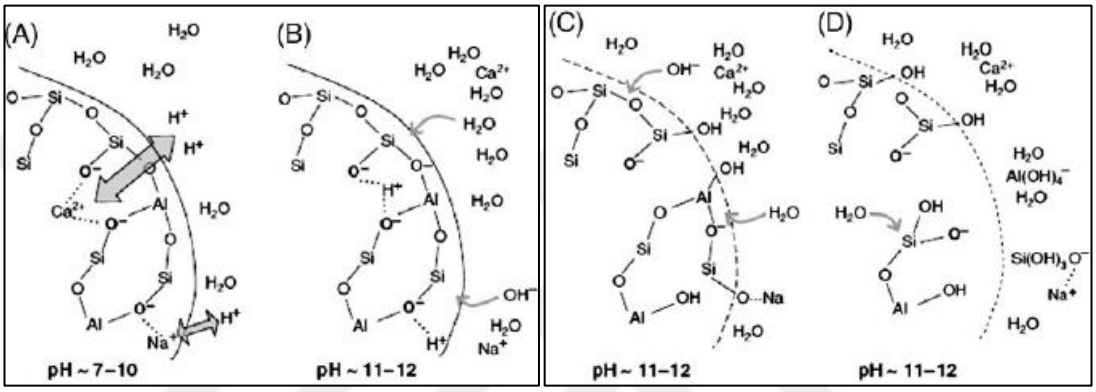


Figure 2.5. Alkaline Activation of calcium-bearing system [53].

Alkali-activated slag is an example of aluminosilicates based on the calcium-bearing system. In this form, alkalis effect on the slag particles firstly, and made up to the polycondensation of reaction products that forms the outer layer [54]. Although the reaction products form substantially of the dissolution and precipitation, the reaction occurs on the surface of the formed particles and controlled by the slow diffusion of the ionic structures into the unreacted core at late ages; hence this period transform into the process a solid-state mechanism. As illustrated in Equation 2.4, 2.5, and 2.6, the cation ($R^+$) acts just as a catalyst for the reaction in the early stages of hydration by cation exchange with the $Ca^{2+}$ ions [54].

$$\text{=Si-O- + } R^+ \rightarrow \text{=Si-O-R} \quad (2.4)$$

$$\text{=Si-O-R + OH-} \rightarrow \text{=Si-O-R-OH}^- \quad (2.5)$$

$$\text{=Si-O-R-OH- + } Ca^{2+} \rightarrow \text{=Si-O-Ca-OH + } R^+ \quad (2.6)$$

Anion types in solution play a key role in the inactivation process, especially at early ages and in different environments [55]. Similar to the cement hydration, the alkali slag reactions end with C-S-H products, with the reaction's intensity being the main difference. Slag also exhibits pozzolanic activity in the presence of $Ca(OH)_2$. So, as can be seen in Figure 2.6, three distinct reactions apparent in a PC and slag blend: cement hydration, slag hydraulic response, and slag pozzolanic reaction [56].

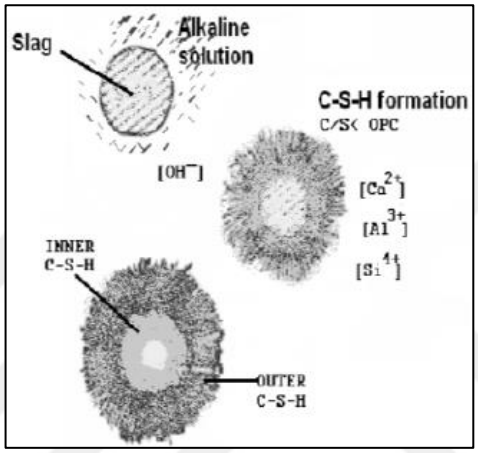


Figure 2.6. The descriptive model of C-S-H [54].

### 2.2.2.2. Alkaline Activators

Many types of alkalis can activate alumina silicate formed materials, and commonly alkaline salts or/and caustic alkalis are used as alkaline activators [57]. Based on their chemical structures, alkali activators can be classified into the six categories as shown in Table 2.1 [33]. Most metallic materials used for the activation process are based on potassium and sodium; however, sodium is mostly used because of its cost. Silicates and hydroxides forms of these matters are the most alkalis [57].

Table 2.1. Groups of Alkaline Activators.

| **Alkaline Activator** | **Chemical Formula** |
|---|---|
| Hydroxides | MOH |
| Non-silicate weak acid salts | $M_2CO_3$, $M_3PO_4$, MF |
| Silicates | $M_2O.nSiO_2$ |
| Aluminates | $M_2O.nAl_2O_3$ |
| Aluminosilicates | $M_2O.\ nAl_2O_3.(2\text{-}6)\ SiO_2$ |
| Non-silicate strong acid salts | $M_2SO_4$ |
| M-Metal | |

**Alkali Silicates**

Sodium silicates ($Na_2O.nSiO_2$), alkali silicate-based materials, is by far the most utilized activation material to prepare AAM. The properties of an activator can be improved by changeable n ratios of silicates. Sodium silicates are available in solid and liquid forms. The commercial name of the liquid form is water glass. Many grades for this material can be characterized by their silica modulus ($SiO_2$-to-$Na_2O$ (or $K_2O$) ratio), which varies from 1.6 to 3.3. This activator has been reported as the most effective activator for producing AAM [58,59]. Sodium silicates have a lower viscosity than potassium silicates. However, potassium silicates are not preferable to use as activators because of expensive [60].

**Alkali Hydroxides**

Alkali metal cations with the hydroxide ($OH^-$) anion are known as alkali hydroxides and most activators are of this type. Potassium and sodium hydroxides are most used in AAM. However, like alkali silicates, sodium-based hydroxides are commonly utilized because of cheaper than potassium-based hydroxides. As alkali hydroxides are diluted in the solution or water, heat of alkali solution is increase [61]. If this activator is utilized more than required, it produces a significant amount of carbonation. The optimum amount has to be determined to avoid carbonation [60].

#### 2.2.2.3. Pozzolanic Sources (Precursors)

Pozzolanic materials are usually alumina silicate-formed materials that have little or no cementitious behavior, but which will, in finely ground form and in the presence of moisture, react chemically with calcium hydroxide at ordinary temperature to form C-S-H [22]. There are two pozzolanic material sources such as natural and by-products. Fly ash, slag, rice husk ash and the other industrial wastes are by-products pozzolans. Metakaolin, volcanic tuff and ash, heated clays are natural pozzolan.

**Fly ash (FA)**

Fly ash (FA) is a byproduct from coal burning production in thermo-electrical industry, and it is rich in silicon dioxide ($SiO_2$) and calcium oxide (CaO). To enhance the compressive strength, chemical resistance, and physical durability of concrete, FA is frequently added as a supplement to PC in the manufacturing of concrete [62]. FA is classified by ASTM C618 into two classes depending on the coal-components as class F and class C [63]. The amount of calcium oxides present in the FA is the primary determinant of the two FA classifications. According to ASTM C618, class C FA has more than 10% CaO [63]. Both classes of FA can be used in producing AAM.

**Slag**

Slag is a by-product derived from Steel&Iron industry and it has a high amount of calcium with silicon dioxide and aluminum dioxide. The chemical components and properties can vary depending on the metallurgical source [64]. Iron blast-furnace slag is the most common type of slag in producing AAM [65].

## 2.3. CHEMICAL ADMIXTURES

AAM has a rapid setting time and low workability due to the high viscosity of the sodium silicate solutions. More water is needed in the fresh mixes to improve workability; however, in this way, the activator concentration reduces leading to a

decrease in the strength and lowering the compressive strength [66]. Therefore, chemical admixtures are required for more workability in the fresh mix. Chemical admixtures are defined as materials added to the concrete at the mixing stage to improve some properties, such as the fluidity, setting behavior, and water requirement for the fresh mix. Chemical admixtures are the last component of a concrete mix that is added to the batch with water at the beginning, middle, or end of the mixing process [67].

### 2.3.1. The Functions and Types of Chemical Admixtures

Liquid or powder-formed chemical admixtures can be added to the mixture at the very beginning or very end of the mixing process [68]. Both conventional concrete and AAM mixes need to meet specific performance criteria [68,69] related to strength, workability, durability, waterproofness, and abrasion resistance. To obtain these characteristics, chemical admixtures must be utilized in some applications. There are several reasons for using admixtures such as cutting down on the overall price of construction, increasing the efficiency with which certain properties can be achieved in the mixes, and preserving the quality of the concrete in mixing, transporting, placing, and curing. The ACI Committee E-701 defines admixtures as follows [67] based on their intended purpose:

There are many types of chemical admixtures utilized to achieve the desired physical and mechanical properties, and each type enhances one or more properties. These are most commonly used in modern concrete technology [67], and There are eight types for this family group according to the ASTM C494 specification as follows:

- Type A – Water-reducing admixtures.
- Type B – Retarding admixtures.
- Type C – Accelerating admixtures.
- Type D – Water-reducing and retarding admixtures.
- Type E – Water-reducing and accelerating admixtures.
- Type F – Water-reducing, high-range admixtures.

- Type G – Water-reducing, high-range, and retarding admixtures.
- Type S – Specific performance admixtures.

Table 2.2. Functions of Chemical Admixtures

| NO | Function |
|---|---|
| **1** | Increase workability without increasing water content or decreasing the water content at the same workability. |
| **2** | Retard or accelerate the initial time of setting. |
| **3** | Reduce or prevent shrinkage or create slight expansion. |
| **4** | Modify the rate or capacity for bleeding. |
| **5** | Reduce segregation. |
| **6** | Improve pumpability. |
| **7** | Reduce the rate of slump loss. |
| **8** | Retard or reduce heat evolution during early hardening. |
| **9** | Accelerate the rate of strength development at early ages. |
| **10** | Increase strength (compressive, tensile, or flexural). |
| **11** | Increase durability or resistance to severe conditions |
| **12** | of exposure, including the application of deicing salts and |
| **13** | other chemicals. |
| **14** | Decrease permeability of concrete. |
| **15** | Control expansion is caused by the reaction of alkalis with reactive aggregate constituents. |
| **16** | Increase the bond of concrete to steel reinforcement. |
| **17** | Increase the bond between existing and new concrete. |
| **18** | Improve impact and abrasion resistance. |
| **19** | Inhibit corrosion of embedded metal. |
| **20** | Produce colored concrete or mortar. |
| **21** | Aid in achieving sustainability requirements. |

#### 2.3.1.1. Water-Reducing Admixtures

Workability can be improved without increasing the water content of freshly mixed concrete by adding water-reducing admixtures, or workability can be maintained with a smaller volume of water. Melamine formaldehyde sulfonate, lignosulfonate, Naphthene sulfonate and polycarboxylate based superplasticizers are commercial in the world, but Naphthene sulfonate and polycarboxylate based superplasticizers are commonly used chemical admixture in water-reducing admixtures [67]. A water-reducing agent causes enhancement of fluidity of the mixture without more water content [70]. Water-Reducing Admixtures typically decrease the water content of a mix by 5 to 10%. This proportion varies with the dosage of the cement and other

components employed [71]. F and G types of admixtures are superplasticizers or high-range water-reducing (HRWR) admixtures. These admixtures significantly reduce the amount of water in a mixture, increase its flowability without leading to excessive set retardation or air entraining in the cement. HRWRs reduce the amount of water in a mixture by as much as 30% [69].

#### 2.3.1.2. Sulfonated Melamine Formaldehyde (SMF)

Sulfonated Melamine Formaldehyde (SMF) is a white powder polymer used in cements and plaster-based formulations, a highly effective water-reducing chemical admixture, used to improve the workability of fresh SGPs without increasing the amount of water. In concretes, addition of SMF in an appropriate mix design results in lower porosity, higher mechanical strength, and an improved resistance to aggressive environments. Using SMF in mixtures results in little or no delay in setting time. Therefore, they are very efficient where early strength is more necessary at low temperatures. Generally, SMF gives no staining in the case of white concrete and gave a good finish.

#### 2.3.1.3. Polycarboxylate Ether (PCE)-Based Superplasticizer

Polycarboxylate (PCE) has recently replaced high-range water reducers. PCE's molecule structure resembles a honeycomb, which allows it to reduce water content without effect curing time. Since PCEs are pricey per liter but extremely potent, they are often utilized at a much lower concentration. PCEs have quickly become the industry leader in pre-cast, and they also often provide water savings of 20-35% when used in self-compacting concrete.

## 2.4. RELATION BETWEEN YIELD STRESS, SHEAR, COHESION AND VISCOSITY OF GEOPOLYMER PASTE (BINGHAM EQUATION)

Fresh geopolymer pastes and cement pastes can be viewed as suspensions of particles such as Fly ash, and GGBFS in continuous fluid-like alkaline solutions. Newtonian, shear thinning, and shear thickening behaviors are observed in the

steady-state flow of cement suspensions with increasing apparent viscosity with shear rate. The electrostatic and Van der Waals forces in colloids, the hydrodynamic forces in liquids, and the contact forces between particles all play a role in determining these three characteristics [72, 73]. These interactions allow cement suspensions to withstand stresses given by the Bingham model:

$$\tau=\tau_y+\eta\,\gamma \tag{2.7}$$

Where, $\tau_y$ is the yield stress, $\eta$ the apparent viscosity, and $\gamma$ the shear rate.

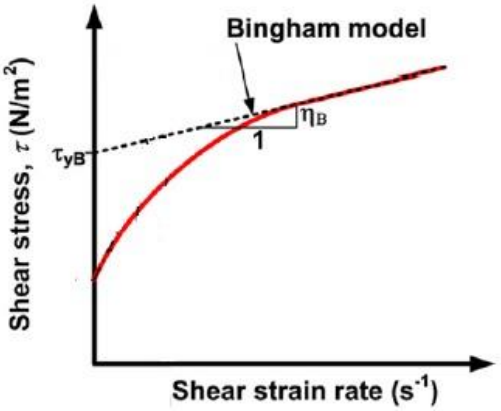


Figure 2.7. The behavior of mudflow with the Bingham model [74].

### 2.4.1. Rheology

The study of rheology governs the behavior of flows [75]. Generally, the Newtonian model is dependent on two rheological parameters, namely, the yield stresses ($\tau_y$) and the viscosity ($\eta$), whereas Newtonian fluids only use parameter $\eta$. Values for both $\tau_y$ and $\eta$ can be obtained with a viscometer. If the mobilized shear stress ($\tau$) is lower than $\tau_y$, then the soil is in a plastic state. Otherwise, the soil is in a viscous liquid state [76].

#### 2.4.1.1. Yield Stress and Viscosity

Figure 2.8. shows a nonlinear curve for real mud flow behavior in the $\tau_y$ and $\gamma$ planes [77]. The $\tau_y$ parameter indicates the minimal shear stress required to cause motion. O'Brien and Julien (1988) stated that $\tau_y$ is similar to cohesion (c) [78]. The value for $\tau_y$ can be derived from viscometry data having similar or different $\eta$ (Ferraris and Winpigler, 2000), which implies that $\tau_y$ is constant for water content [79]. Viscosity ($\eta$) describes fluid stiffness and measures the resistivity of fluid to flow or can be defined as an efficient parameter in explaining the initiating factors associated with starting the mudflow or geopolymer paste. The gradient line at a particular point in Figure 2.8 is $\eta$. Therefore, $\eta$ is defined as the shear stress required for a fluid to pass from one layer to another for a specific distance away from the original position of the fluid with unit velocity [80].

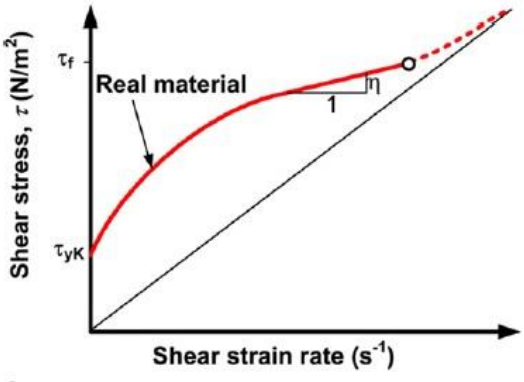


Figure 2.8. The behavior of mudflow with the model for real material [74].

Figure 2.9. represents the apparent viscosity as a function of the shear rate for geopolymer paste ($H_2O/Na_2O$ = 15) and cement paste (W/C =0.35). The graphic illustrates the difference between the viscosity of a common MK-based geopolymer and that of cement paste. Geopolymer has a lower viscosity than the cement does over a broad range of shear rates. Additionally, unlike cement paste, the viscosity appears to be dominated by a viscous contribution rather than a colloidal one [81].

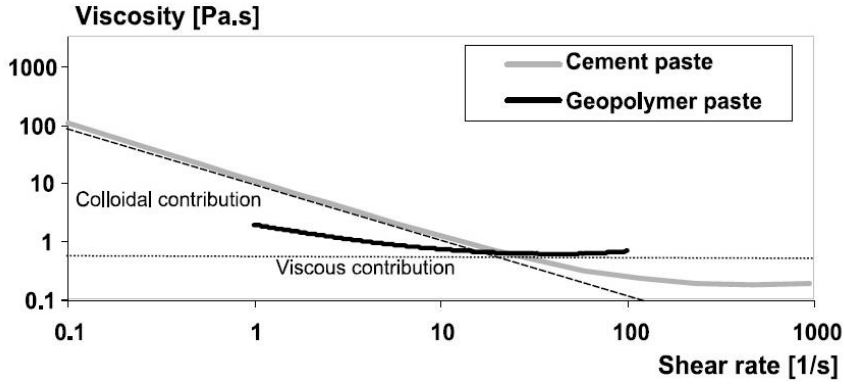


Figure 2.9. Apparent viscosity versus shear rate for geopolymer paste and cement paste [81].

#### 2.4.1.2. Shear Thinning

For actual materials, fluid deformation can take the form of either shear thickening or shear thinning. When both increasing, shear thickening occurs, but if an increase is followed by a drop in, shear thinning happens instead. This latter reaction is typical of soil in its natural state [82]. Flow curves with a negative gradient [83] depict the link between shear thickness and shear rate on a log-log scale, providing visual evidence of the phenomenon.

#### 2.4.1.3. Non-Newtonian Flow

The fluids utilized in the drilling industry are mostly non-Newtonian, except for a few well-understood Newtonian fluids like water, air, and some oil products [84]. To characterize the flow properties of non-Newtonian fluids, numerous rheological models have been put forth. According to the Bingham model, flow happens when non-Newtonian fluids have a driving force larger than their yield stress [85]. In the presence of low shear rates, the power-law model adequately describes the flow properties of non-Newtonian fluids [86]. Since the Carson model's rheological curve is a straight line, it may be used to predict the rheological properties of non-Newtonian fluids at high shear rates based on measurements taken at low and medium shear rates [87]. The three-parameter Herschel-Bulkley model accurately describes the rheological properties of non-Newtonian fluids over a wide range of

shear rates [88]. The Nasiri-Ashrafizadeh model extends the Herschel-Bulkley model by including a fourth parameter to better characterize non-Newtonian fluids [89].

All fluids with a yield point or an asymmetric shear stress-shear rate connection are considered non-Newtonian. The dynamics of flows that deviate from Newtonian behavior can be described using nonlinear approximations based on the power law. According to American Standard API 13B [90], the Herschel-Bulkley correlation is the primary flow model for bentonite suspensions. There are three variables used in the Herschel-Bulkley model of fluid motion [91]: flow index n, consistency index C, and yield point $\tau_0$, see the equation below.

$$\tau=\tau_0+C\gamma^n \quad (2.8)$$

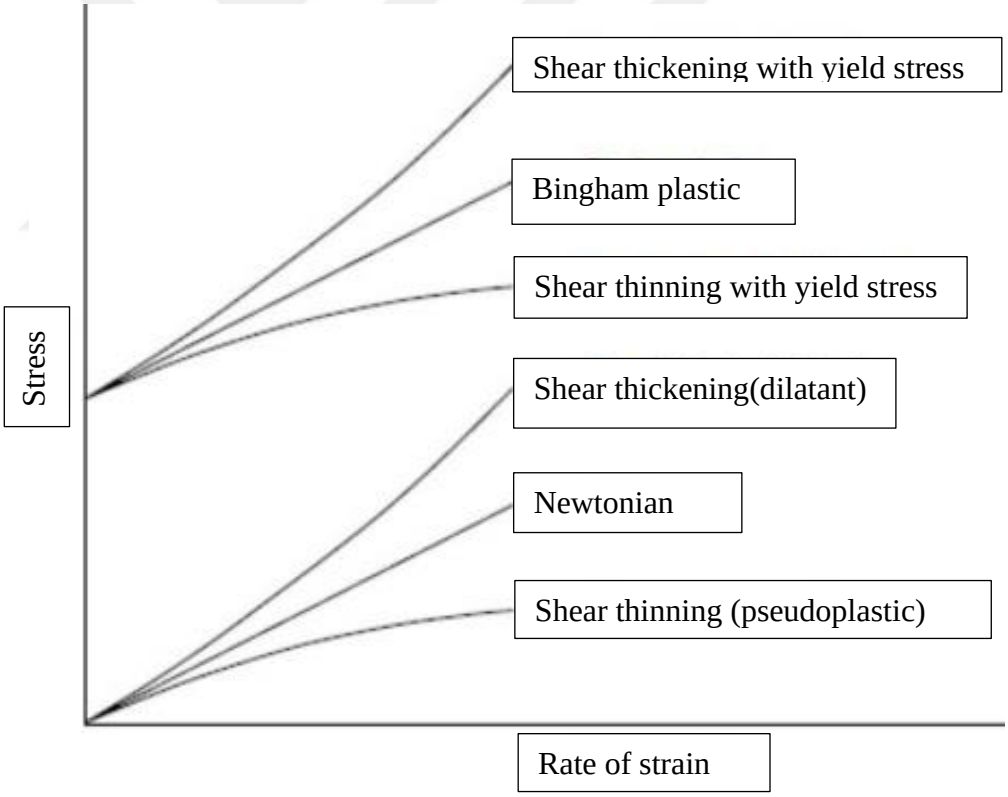


Figure 2.10. The six main classes of time-dependent fluids are presented in flow curves of stress against strain rate in shear flow [92].

The Herschel-Bulkley model can also be used to characterize the flow of non-Newtonian fluids as well as those of Newtonian fluids. When compared to experimental rheological data, the model's predictions are reliable and accurate. The

Herschel-Bulkley model can be used to predict the six basic types of flow curves shown in Figure 2.10, given appropriate boundary conditions:

For $\tau_0 = 0$ and $n < 1$ shear thinning behavior (pseudoplastic)
For $\tau_0 = 0$ and $n = 1$ Newtonian behavior
For $\tau_0 = 0$ and $n > 1$ shear thickening behavior (dilatant)
For $\tau_0 > 0$ and $n < 1$ shear thinning behavior with yield stress
For $\tau_0 > 0$ and $n = 1$ Bingham plasticity
For $\tau_0 > 0$ and $n > 1$ shear thinning behavior with yield stress

About the respective boundary condition, the Herschel-Bulkley model is reduced to common rheological flow models,

Bingham Model [Bingham 1922] using

$$\eta_{pl} = m \text{ and } \tau_B = \tau_0 \tag{2.9}$$

$$\tau = \tau_B + \eta_{pl}\,\gamma \tag{2.10}$$

Power-Law-Model [Metzner 1956] using K= C

$$\tau = K\,\gamma^n \tag{2.11}$$

Newtonian Model [Sochi 2007] using $\eta_v = C$

$$\tau = \eta_v\,\gamma^n \tag{2.12}$$

## 2.5. MARCH FUNNEL AND RELATED STUDIES

Viscosity can be determined by a straightforward “Marsh funnel” tool, which works by timing how long it takes a known volume of liquid to pass from a cone via a small tube. It is standardized for mud engineers to assess the caliber of drilling mud. Flow cones are another type of cone with various geometries and orifice configurations.

The working progress of the Marsh Funnel can be explained as follows: The tube end of the funnel is sealed up with a finger while being held vertically. Pouring the liquid through the mesh will eliminate any debris that could clog the tube before it is measured. The volume within is equal to the rated volume after the fluid level reaches the mesh. A stopped clock is started, the finger is released, and the liquid is allowed to flow into a measuring container to take the measurement. The viscosity is calculated using the time in seconds.

Almahdawi et.al (2014), examined the effect of the March Funnel apparatus on oil viscosity measurements. Instead of using the conventional method, they used the March Funnel for the viscosity measurement of drilling fluids in quality control. The viscosity readings from the funnel are in good agreement with those from the widely used Fann 35 viscometer. Various amounts of bentonite, barite and other additives were used to create a variety of samples.

$$\mu_{app.} = \rho\,(t - 28) \text{ and } \mu_{app.} = -0.0118t^2 + 1.6175t - 32.168 \quad (2.12)$$

where apparent viscosity (μapp.) in (cp), Marsh funnel time (t) in seconds, and the density (ρ) in gm/cm$^3$.

In 1931, [93] Hallan created the Marsh Canal. It is a unit of time measurement for filling a fixed volume with a liquid. (A quarter is the typical US volume.) The rheological qualities of the fluid are related to the rate at which it flows through the narrow end of the funnel. The "viscosity" of a liquid, measured in seconds using a swamp funnel, is a useful measure of its consistency. When filling a quart, more time is needed for a liquid with a higher viscosity. There are 28 seconds added to the Marsh funnel time for every liter of fresh water. Image 1 depicts a typical sink funnel. A sump funnel is a straightforward and reliable method for estimating the thickness of drilling mud. Additional oilfield fluids are used in this application of the funnel.

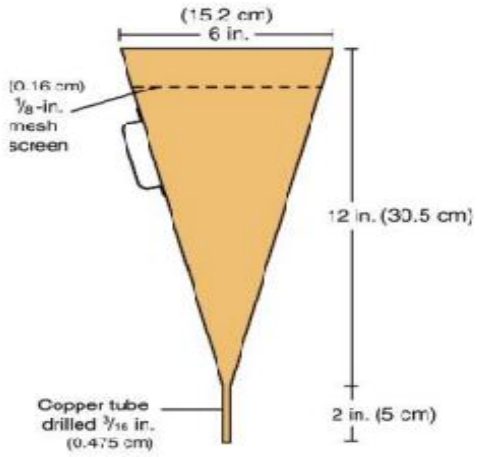


Figure 2.11. Marsh funnel [94].

Even though standard rheometers can be used to determine the rheological properties of these fluids, a more straightforward technique is generally preferred. The purpose of this study is to create such a technique for employing a Marsh funnel to ascertain the rheological properties of non-Newtonian fluids. The rate of drainage of the test liquid can be measured by filling the funnel to a specific height. The flow behavior of Marsh funnels is computed numerically [95]. The simulation yields a broad understanding of the significance of the Marsh funnel time and a correlation for transforming it into an effective viscosity value applicable to non-Newtonian fluids. M.J. Pitt's ultimate formula is as follows:

$$\mu_{eff.} = \rho\,(t - 25) \tag{2.13}$$

Where: μeff. = effective viscosity (cp); ρ= density (gm/cc); t=time (sec.)

Since we relied on experimental data rather than numerical simulations, the model described here may calculate apparent viscosity rather than effective viscosity, both of which depend on Pitt's equation.

## 2.4. LITERATURE REVIEW

Saha S. and Rajasekaran C. (2017) performed an experimental investigation on several methods to enhance the mechanical properties of FA/Slag Based geopolymer

paste. As the amount of GGBFS increased in the mixes, both the initial and final setting times of geopolymer paste decrease dramatically. The compressive strength of geopolymer paste evaluated after 28 days increased as the NaOH solution concentration was increased up to 16 M. GGBFS increasing at 50% in geopolymer paste mixtures caused denser structures and higher strength (78.2 MPa) [96].

Oderji S.Y. et. al (2019) studied the effect of slag amounts and an alkaline activator on the FA-based geopolymer binders. They concluded that adding more slag, a CaO-rich material, increased the compressive and flexural strengths but decreased workability. As FA replacement increase up to 15%, the microcracks grew larger. Optimum FA replacement with slag on the study is 15% to obtain higher mechanical strength and fresh characteristics of the binders [97].

Chattopadhyay et. Al (2019) examined the effect of SP addition on Geopolymer composites. GGBFS was combined with FA. To regulate the workability, SP content for both PCEs and Naphthalene-based was added to geopolymer composite by the flow table test. The ultimate compressive strength is obtained as 46 MPa, bulk density, apparent porosity, and water absorption improve upon the addition of the ideal quantity of slag. The microstructure of the geopolymer composites varied by GGBFS ratios. GGBFS addition leads to the N-A-S-H gel and C-A-S-H gel with N-A-S-H gel formations [98].

Raju T. et al. (2022) studied that as the GGBFS percentage in geopolymer paste increased, the workability and setting time decreased. Ideal replacement of FA with GGBFS is less than 50% in preparing geopolymers for ambient curing. The maximum flow value of FA-based geopolymer paste increase 346.19% according to GGBFS based geopolymer paste. The test findings show that the flow characteristic reduces as the GGBFS content rises. fineness and angular particles of GGBFS is effective on this behavior. Regardless of the type of SP, flow value increases as SP dose (up to 3%) [99].

The properties of fresh and hardened FA/GGBFS blended geopolymer paste and mortar were studied by Samantasinghar S. and Singh S.P. (2019). In geopolymer

composites, from 2M to 16M NaOH is used. Geopolymer mortar made from GGBFS and activated with an 8M NaOH solution has a maximum compressive strength of 44 MPa. The higher the NaOH content, the quicker the scene will set [100].

Widayanti A. et. al. (2018) studied the mechanical properties of FA-based geopolymer paste was conducted. Maximum compressive strength is obtained 98.6 MPa with 8M NaOH concentrations. $Na_2SiO_3$/NaOH: 2.5, 75% FA, and 8M NaOH caused maximum compressive strength value [101].

The microstructure and mechanical characteristics of GPP made from F type FA were investigated by Q. Lv et al. The results show that the unconfined compressive strength of FA-based geopolymer is influenced by the change of modulus ($Na_2SiO_3$) and dosage of sodium silicate. The geopolymer samples improved in strength as the modulus value decreased and the sodium silicate dose increased. An increase in the sodium silicate dosage and a drop in the modulus value sped up the dissolving of fly ash, but they also filled the system's large pores, resulting in fewer large holes and more tiny ones. The compressive strength at 28 days is improved by as much as 16 MPa for geopolymer paste with a (40x40) mm dimension when the modulus value of the sodium silicate is reduced from 3.28 to 1.5 [102].

Mádaı F. et al. (2015) focused on using deposited FA as the primary ingredient in geopolymer. The test specimens were created solely through the geopolymerization of a NaOH liquid. The compressive strength of cylindrical specimens was assessed. Finally, X-ray diffraction, optical, and scanning electron microscopy were used to evaluate samples of the ground FA-based geopolymer specimens. Results demonstrate that it is feasible to produce geopolymers with the required strength from the examined F-type FA. Zeolite-A is visible when comparing the crystalline components for various geopolymer samples, and its amount gradually increases according to XRD data. An analysis using SEM and EDS showed that the interstitial fine-grained matrix has a higher Na content, which had the strongest strength [103].

Dumitru Doru et al (2017) studied the effect of varying the ratio of FA to the alkaline activator and the ratio of $Na_2SiO_3$/NaOH in class F-based geopolymers. The

researchers found that the Si/Al ratio, base material, particle diameters, alkaline activator concentration, calcium quantity, time of synthesis/hardening, and geopolymerization temperatures all had a significant impact on the final geopolymer's properties. A higher percentage of GGBFS in place of FA results in geopolymer mortar with higher compressive strength at 70 MPa [104].

Raju T. et al. (2020) found that the inclusion of SNF into mixtures performed better than PCE regarding mini-slump tests for all the mixes and SNF is more successful at delaying in setting time for pastes containing 100% GGBFS. Regardless of the type of SP, workability increases as SP dosage to 3% [106].

Nematollahi B. and Sanjayan J. (2014) studied on the workability and strength of a class F type fly ash-activated geopolymer paste with various commercial SPs including naphthalene, melamine, and modified polycarboxylate. Naphthalene (N) based SP showed a 136% rise in the relative slump in the case of FA-based geopolymer paste activated by 8M NaOH solution, with no adverse effects on compressive strength. The most effective kind SP is modified polycarboxylate (PC) based SP, relative slump increased in a 39-45% and compressive strength decreased 29% [107].

Laskar M.S. et al (2018) focused an experimental study to ascertain the effect of an alkali activator concentration and a liquid PCE-based SP on a GGBFS/FA-based geopolymer. PCEs-based SP delays the early setting time and enhances the workability of the GGBFS-FA. PCEs-based SP performs better up to a dose of 1.5%. The strength of the geopolymer mixtures increases with the addition of PCE-based SP. However, PCE dosages of more than 0.5% of the total binder content caused a considerable loss in strength [108].

Nuruddin M. F. et al (2011) investigated how the concentration of modified PCE-based SP increased from 8M to 12M, improving the interfacial transition zone (ITZ) and microstructure. Compressive strengths of concrete could have up to 51.52 MPa at 28 days with the addition of a 6% liquid-modified PCEs-based SP [109].

Razak S.A. et al (2020) studied a comparison of OPC Paste with FA-based geopolymer. The results demonstrates that the FA-based geopolymer paste has less porosity than OPC paste in surface area, pore volume, and pore size. When pore size and water absorption are reduced, the compressive strength of FA-based geopolymer can be reached 76.72 MPa at 28 days [110].

Zailani W.W.A. et al (2020) investigated the morphological and mechanical properties of a FA-based geopolymer paste for using as a patching medium on OPC concrete overlay. In the first stage, many geopolymer mixtures were synthesized using NaOH concentrations of 8, 10, 12, and 14 M. According to the results, the setting time decreases with increasing NaOH molarity, from 53 min at 8 M to 30 min at 14 M. The compressive strength of FA-based geopolymer paste was measured at 92.5 MPa after 60 days. The slant shear test result was 11 MPa at 12 M. Setting time was observed to be reduced with increasing NaOH molarity, and this was attributed to the formation of several geopolymer gels, most notably C-A-S-H gel near the interface zone, where the high concentration of calcium cations resides [111].

# PART 3

# MATERIALS AND METHODS

## 3.1. MATERIALS

### 3.1.1. Ground Granulated Blast Furnace Slag (GGBFS)

As a byproduct of the iron production process, limestone, iron ore, and coke are burned to temperatures of up to 1500 $^{o}$C in a blast furnace to create granulated blast furnace slag (GBFS). GBFS is made up of oxides found in limestone and alumina and silicate from iron ore. GGBFS used in this study conformed to ASTM C989 is processed through drying and ground by using a horizontal ball mill into a fine near-white powder given in Figure 3.1. Its particle sizes are observed below 70 μ and most of the particles ($D_{90}$) are below 35 μ as shown in Figure 3.2. According to the laser particle size analysis method, the specific surface area of GGBFS is 0.74 $m^2/g$.

Figure 3.1. Ground granulated blast furnace slag (GGBFS).

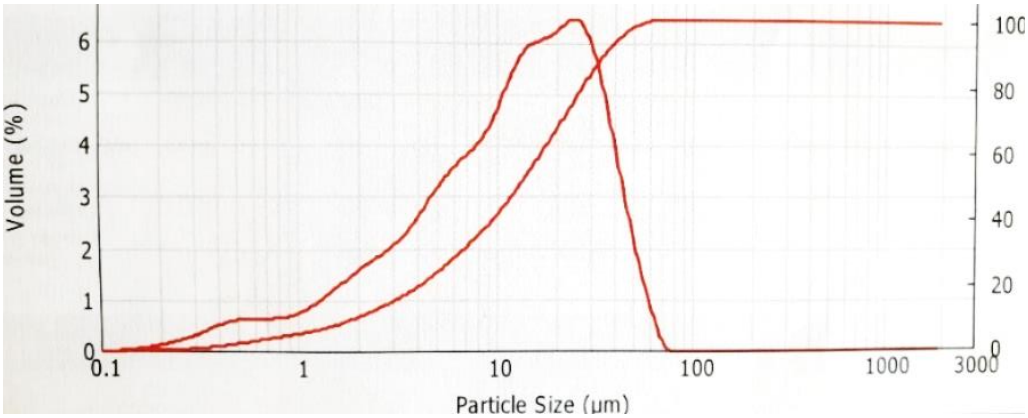


Figure 3.2. Particle size analysis of GGBFS by using laser particle sizer method.

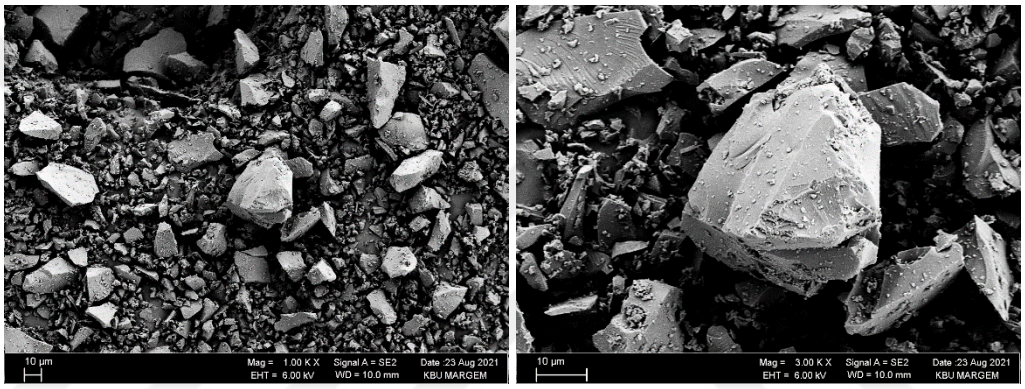


Figure 3.3. SEM images of GGBFS.

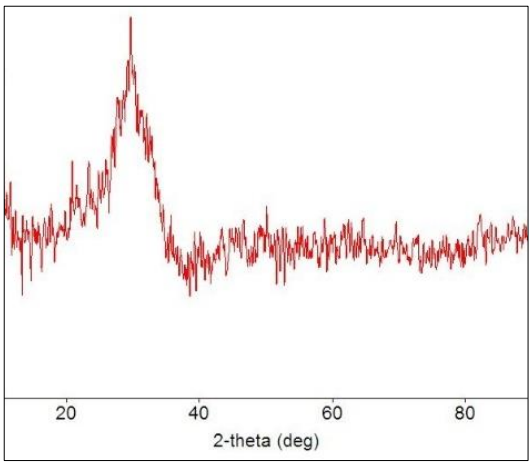


Figure 3.4. XRD pattern of GGBFS.

The chemical and physical properties of GGBFS are shown in Table 3.1. According to the SEM images given in Figure 3.3, the grain sizes are less than 50 µ and also its

structure and shape are amorphous and sharp/angular, respectively. From the XRD pattern, as shown in Figure 3.4, it was observed that GGBFS is composed of amorphous calcium, alumina-silicate structure.

### 3.1.2. Energy Transferred System Ash (ETS)

Like low calcium fly ash (Type F) (Energy Transferring System ash derived from Ferrite -steel industry –ETS) with a dark color appearance collected from the thermal power plant as shown in Figure 3.5, compatible with ASTM C168 was used for production slag-based geopolymer paste (SGP). The physical and chemical compositions of ETS are shown in Table 3.1. As shown in Figure 3.6 obtained from SEM analysis of ETS, it was seen spherical grains with a grain size of approximately 80 microns, mostly amorphous and angular/spherical in structure, slightly similar to thermal power plant F type FA.

Figure 3.5. ETS ash.

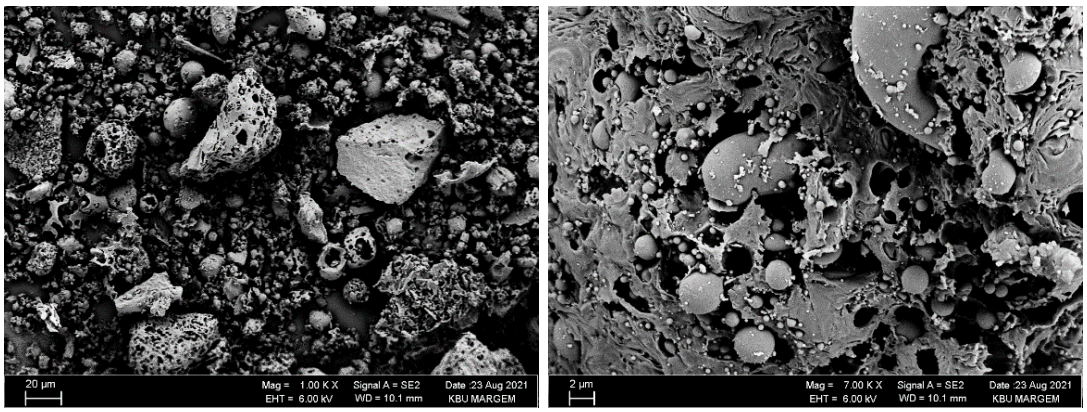


Figure 3.6. SEM images of ETS ash.

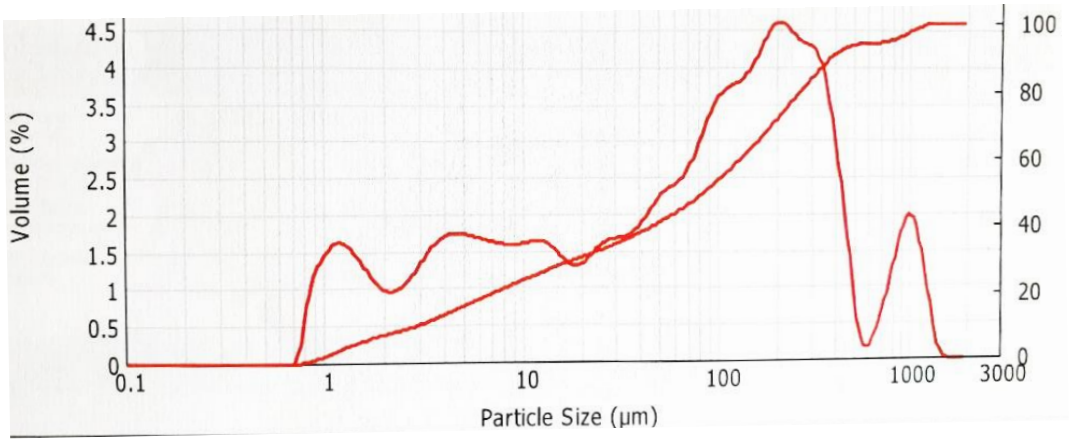


Figure 3.7. Particle size analysis of ETS ash by using laser particle sizer method.

Particle size analyses of ETS ash were conducted by using a laser particle sizer (Mastersizer 3000) and the analysis result was given in Figure 3.7. According to Figure 3.7, the maximum size of the ETS ash is almost 1 mm and most of the particles ($D_{90}$) are below 394 µ. So, the particle size of ETS ash is bigger than the GGBFS. Moreover, according to the particle size analysis, the specific surface area of the ETS ash is 0.689 $m^2/g$. The specific surface areas of GGBFS and ETS ash are slightly similar.

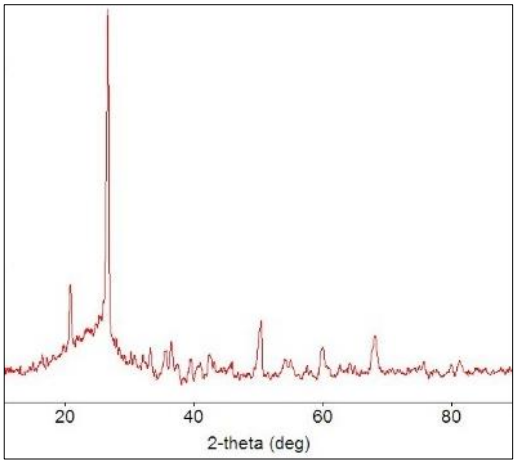


Figure 3.8. XRD pattern of ETS ash.

According to the XRD pattern of ETS ash given in Figure 3.8, high silica content, calcium, and aluminum peaks were detected. Quartz, calcite, tridymite, and clayey structure were also observed as mineral structures.

Table 3.1. Physical properties and chemical composition of GGBFS, ETS ash.

| **Oxides** | **ETS ash** | **GGBFS** |
|---|---|---|
| $SiO_2$ | 50.74 | 40.4 |
| $Al_2O_3$ | 28.01 | 10.6 |
| $Fe_2O_3$ | 7.998 | 1.28 |
| CaO | 5.435 | 34.19 |
| MgO | 2.114 | 7.63 |
| $SO_3$ | 0.768 | 0.68 |
| $K_2O$ | 1.120 | 2.4 |
| $Na_2O$ | 1.364 | 0.17 |
| $Cl^-$ | 0.100 | |
| Loss of ignition (LOI) | 2.07 | 2.74 |

### 3.1.3. Alkaline Activated Solution

The polymerization process required an alkaline activator. Generally, the most common alkali-activated solutions are a combination of (NaOH) and ($Na_2SiO_3$) to start the activation of reactions [112]. Dissolved sodium silicate ($Na_2SiO_3$) in solution gives rise to the reactions faster than hydroxide solution, also it's cheaper in comparison with potassium silicate ($K_2Si_2O_5$), so $Na_2SiO_3$ is recommended to use during alkaline liquid preparation in common [113]. Table 3.2 shows the chemical compositions and physical properties of $Na_2SiO_3$ used in this study. However, NaOH is used for reacting silicate (Si) and aluminum (Al) by adding $Na^+$ ion, which is used in the process of polymerization. In this study, sodium silicate ($Na_2SiO_3$) solution with/without 10 M of sodium hydroxide (NaOH) in different proportions was utilized and mixed as an alkaline-activated solution in order to activate the ETS ash and GGBFS. To prepare 10 M of NaOH liquid, the NaOH pellets were dissolved in distilled water (400 g NaOH and water in 1 lt volume) as shown in Figure 3.7

Table 3.2. The Chemical and physical properties of $Na_2SiO_3$.

| | |
|---|---|
| Density ($g/cm^3$) | 1.396 – 1.418 |
| $Na_2O$ (wt%) | 11.3 – 12.9 |
| $SiO_2$ (wt%) | 22.6 – 25.8 |
| Module ($SiO_2$/ $Na_2O$) | 1/2 |

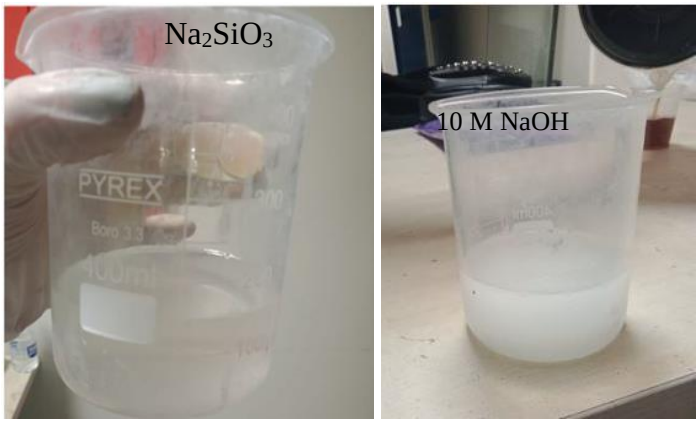


Figure 3.9. Preparation of alkaline activators.

### 3.1.4. Chemical Admixtures

#### 3.1.4.1. Sulfonated Melamine Formaldehyde (SMF)

In this study raw powder form Sulfonated Melamine Formaldehyde (SMF) as shown in Figure 3.10 were used. Table 3.5 shows the technical properties of SMF complies with ASTM C-494 type A and F.

Table 3.3. Technical properties of used SMF.

| **Properties** | **SMF** | **PCE** |
|---|---|---|
| Appearance | white powder | White Powder |
| Purity | 99.8%≤ | 99%≤ |
| Moisture | ≤ 0.1% | |
| PH Value | 7.5-9.5 | 5-7 |
| Water Reducing Ratio | 12%≤ | 28%≤ |
| Chloride content | | ≤ 0.10% |
| Ash | ≤ 0.03% | - |
| Haze Degree | ≤20 | - |
| Color Degree | ≤20 | - |

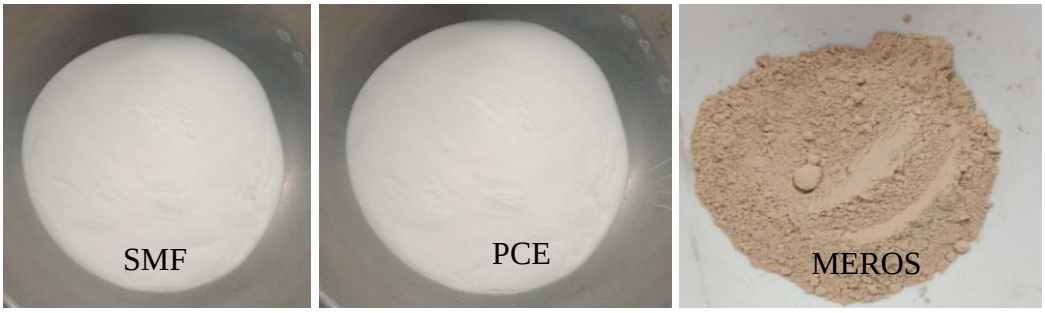


Figure 3.10. Chemical admixtures used in this study.

### 3.1.4.2. Polycarboxylate Ether (PCE)-Based Superplasticizer

In this study, raw powder form Polycarboxylate ether-based superplasticizer, as shown in Figure 3.10 complies with the requirement of ASTM C494 were used. Technical properties of PCE-based superplasticizers are given in Table 3.3.

### 3.1.4.3. MEROS (Maximized Emission Reduction of Sintering) Ash

The MEROS technology is a process that exemplifies the reduction of maximized emission of sintering, which is a dry type of gas cleaning technique to decrease harmful emissions from sinter plants. In a set of successive processing steps, the organic and harmful metallic components and dust are removed from the sinter-off gas to levels earlier unattained with traditional gas processing techniques. In several attempts, the economic and technical benefits of this innovative process of sinter off gas-cleaning were confirmed. This technique was adopted by the construction of the world's first MEROS industrial plant with rose at the Voestalpine Stahl's sinter plant, Linz/Austria. MEROS ash as shown in Figure 3.10 is a chemical admixture used in alkali-activated ETS/GGBFS-based mixtures as water reducers. In preliminary trials, MEROS ash was dissolved up to 10% by weight in water and $Na_2SiO_3$ at room temperature, and up to 30% by weight in 10 M of NaOH and $Na_2SiO_3$ at 80 °C temperature. In experimental studies, the MEROS ash is used either as a compound or in terms of solubility to support the activators by dissolving up to 20%. Table 3.3 shows the chemical composition (metal analysis) of MEROS ash, which was conducted in the Iron&Steel Institute laboratories. Whereas Table 3.4 represents the results of the non-destructive analysis of MEROS ash, which are X-Ray fluorescence

(XRF) and X-Ray diffraction (XRD), respectively. The SEM analysis for MEROS ash given in Figure 3.11 the grain sizes are less than 50 microns, amorphous and angular.

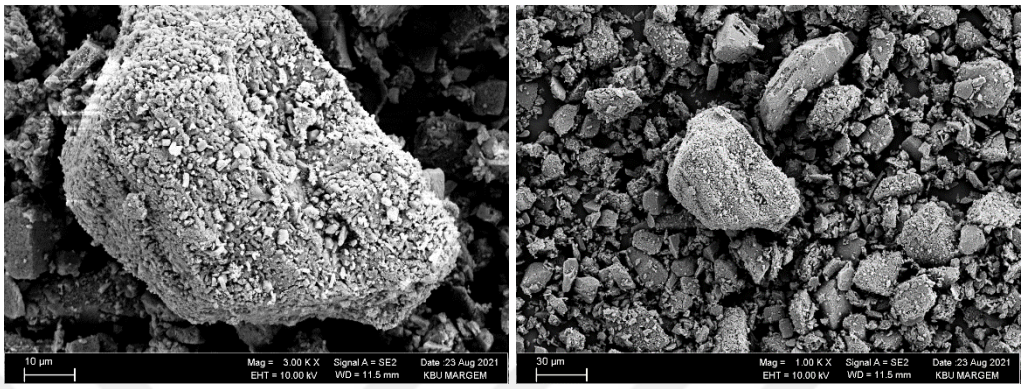


Figure 3.11. SEM images of MEROS.

As shown in Figure 3.12, the XRD pattern of MEROS ash, sodium carbonate, and sodium sulfate structures was observed. Thenardite and Nahcolite structures were also detected as a mineral structure.

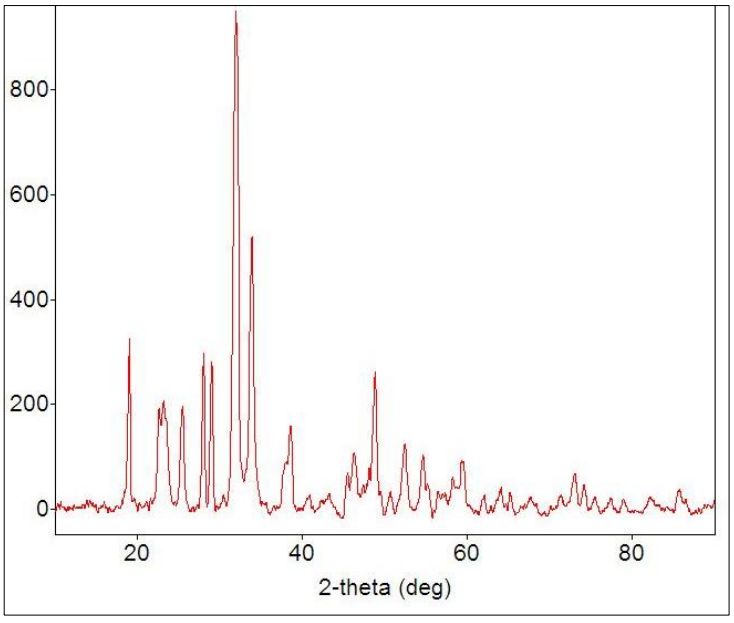


Figure 3.12. XRD pattern of MEROS.

Table 3.4. Chemical composition and metal analysis of MEROS ash.

| Ingredients | mg/Kg | Ingredients | mg/Kg |
|---|---|---|---|
| Na | 440 | Mg | 260 |
| Al | 470 | Mn | 160 |
| Cu | 460 | As | 2.1 |
| Zn | 320 | Pb | 1.0 |

Table 3.5. Results of XRD and XRF investigation of MEROS ash.

| X-ray diffraction (XRD) | | X-ray fluorescence (XRF) | |
|---|---|---|---|
| **Components** | **%** | **Components** | **%** |
| Sodium sulfate $Na_2(So_4)$ | 77 | Sodium Sulfate $Na_2So_4$ | 85 |
| Thenardite, Syn $Na_2So_4$ | 5 | Sodium Carbonate $Na_2co_3$ | 1.5 |
| Nahcolite, Syn $NaHco_3$ | 17.6 | Sodium Chloride Nacl | 7.2 |
| - | - | Sodium Fluoride NaF | 1 |

## 3.1. EXPERIMENTAL STUDY

In the experimental study, 2 different stages were performed: fresh and hardened state studies. In the first stage of this study, the main purpose is to determine the effects of chemical admixtures on SGPs. Hence, solution/powder ratios of SGPs were selected quite high as 1.2 due to obtaining of flowability of the pastes efficiently. Because in this stage March funnel was used to determine the viscosity of the pastes associated with the flow table and final setting times. To appear in the flow function of SGPs was too difficult because of the higher cohesiveness of particles, so the higher S/P ratio was selected for to flow of pastes. In addition, primary studies showed that the minimum S/P ratios required higher than 1.2, because of their effective flowability appearance. In this stage, the compressive and flexural strength tests were conducted at the age of 7, 28, and 90 days.

The second phase of this research focused on determining whether SGPs prepared with chemical admixtures at a lower S/P ratio have a higher compressive strength. Therefore, only 50x50x50 mm cubes of paste were prepared and examined on day 2 and day 28 under laboratory condition. On the $28^{th}$ day, X-Ray Diffraction Analysis (XRD), Energy Dispersive X-Ray Spectroscopy (EDS), and scanning electron microscope (SEM) analyses were performed to inspect SGP specimens.

### 3.1.1. Mix Design Parameters and Preparing of SGP Specimens

The applicable mix design of ETS ash /slag-based geopolymer pastes activated by $Na_2SiO_3$ and $Na_2SiO_3$+10M NaOH solutions in different percentages needs a balance between economy and strength-workability-density-durability. In this study, many parameters were adopted such as solution/powder ratio, the molar concentration of NaOH, curing ages at 7, 28, and 90 days, $Na_2SiO_3$ to NaOH ratio, and types of SPs. Therefore, the mixture design of ETS ash/slag based SGPs were given in Table 3.6. Additional definitions about Tablo 3.6 are given in Figure 3.13 and 3.14.

In all stages, initially, activator solutions were prepared by adding chemical admixtures (SMF, MEROS ash, PCE) separately to the solutions, and they were blended till a homogenous solution appeared. Afterward, ETS ash and GGBFS were added to the solution and mixed into the mixer for at least 7 min. Several experiments were carried out on fresh state SGPs according to the standards set forth by the American Society for Testing and Materials (ASTM), including Marsh funnel, Setting time, and flow table tests. Then the fresh SGPs were poured into prismatic and cubic molds with sizes 40x40x160 mm and 50x50x50 mm to determine the compressive strengths and flexural strength of SGPs on $7^{th}$, $28^{th}$ and $90^{th}$ days, respectively (see Figure 3.13). In the meanwhile, SGPs were cured at 80 °C for 3 h and then placed in the laboratory in ambient conditions till test days.

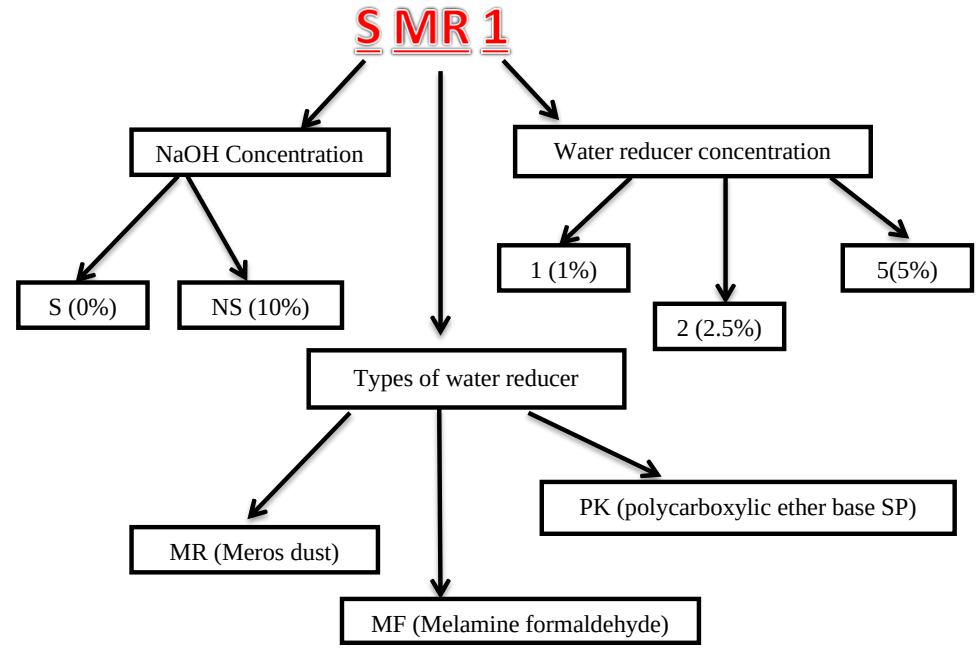


Figure 3.13. The description of each mixture symbol for first step.

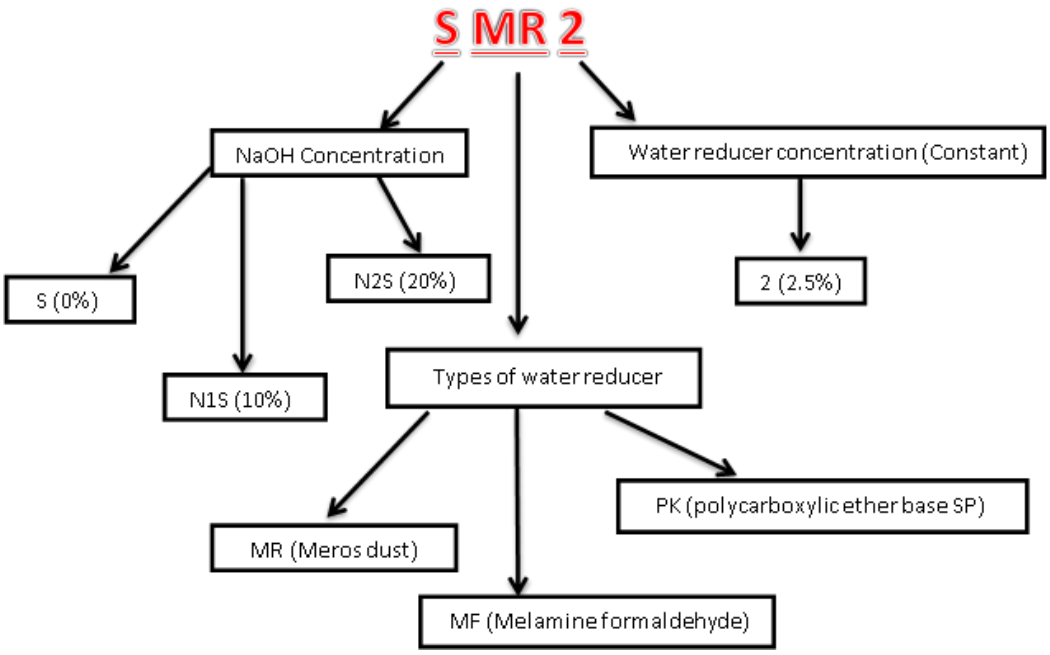


Figure 3.14. The description of each mixture as a second step.

Table 3.6. Mix design of SGPs.

| Code | Compounds percentage (by weight) | | | | | S/P ratio | Molar concentratio | NaOH (10M) / $Na_2SiO_3$ | Bulk Density |
|---|---|---|---|---|---|---|---|---|---|
| | GGBFS | ETS ash | NaOH (10M) | $Na_2SiO_3$ | SP (%) | | | | |
| **The first stage of the study** | | | | | | | | | |
| E0 | 0.15 | 0.30 | 0.00 | 0.55 | 0 | 1.20 | 4.2 | 0/100 | 1.69 |
| EMR5 | 0.15 | 0.30 | 0.00 | 0.55 | 5 | 1.20 | 4.2 | 0/100 | 1.72 |
| S0 | 0.30 | 0.15 | 0.00 | 0.55 | 0 | 1.20 | 4.2 | 0/100 | 1.75 |
| SMR1 | 0.30 | 0.15 | 0.00 | 0.55 | 1 | 1.20 | 4.2 | 0/100 | 1.76 |
| SMR2 | 0.30 | 0.15 | 0.00 | 0.55 | 2.5 | 1.20 | 4.2 | 0/100 | 1.77 |
| SMR5 | 0.30 | 0.15 | 0.00 | 0.55 | 5 | 1.20 | 4.2 | 0/100 | 1.79 |
| SMF1 | 0.30 | 0.15 | 0.00 | 0.55 | 1 | 1.20 | 4.2 | 0/100 | 1.76 |
| SMF2 | 0.30 | 0.15 | 0.00 | 0.55 | 2.5 | 1.20 | 4.2 | 0/100 | 1.77 |
| SMF5 | 0.30 | 0.15 | 0.00 | 0.55 | 5 | 1.20 | 4.2 | 0/100 | 1.79 |
| SPK1 | 0.30 | 0.15 | 0.00 | 0.55 | 1 | 1.20 | 4.2 | 0/100 | 1.76 |
| SPK2 | 0.30 | 0.15 | 0.00 | 0.55 | 2.5 | 1.20 | 4.2 | 0/100 | 1.77 |
| SPK5 | 0.30 | 0.15 | 0.00 | 0.55 | 5 | 1.20 | 4.2 | 0/100 | 1.79 |
| NS0 | 0.30 | 0.15 | 0.05 | 0.50 | 0 | 1.20 | 8.1 | 10/90 | 1.75 |
| NSMR1 | 0.30 | 0.15 | 0.05 | 0.50 | 1 | 1.20 | 8.1 | 10/90 | 1.76 |
| NSMR2 | 0.30 | 0.15 | 0.05 | 0.50 | 2.5 | 1.20 | 8.1 | 10/90 | 1.77 |
| NSMR5 | 0.30 | 0.15 | 0.05 | 0.50 | 5 | 1.20 | 8.1 | 10/90 | 1.79 |
| NSMF1 | 0.30 | 0.15 | 0.05 | 0.50 | 1 | 1.20 | 8.1 | 10/90 | 1.76 |
| NSMF2 | 0.30 | 0.15 | 0.05 | 0.50 | 2.5 | 1.20 | 8.1 | 10/90 | 1.77 |
| NSMF5 | 0.30 | 0.15 | 0.05 | 0.50 | 5 | 1.20 | 8.1 | 10/90 | 1.79 |
| NSPK1 | 0.30 | 0.15 | 0.05 | 0.50 | 1 | 1.20 | 8.1 | 10/90 | 1.76 |
| NSPK2 | 0.30 | 0.15 | 0.05 | 0.50 | 2.5 | 1.20 | 8.1 | 10/90 | 1.77 |
| NSPK5 | 0.30 | 0.15 | 0.05 | 0.50 | 5 | 1.20 | 8.1 | 10/90 | 1.79 |
| **The second stage of the study** | | | | | | | | | |
| S0 | 0.43 | 0.22 | 0.00 | 0.35 | 0 | 0.54 | 4.2 | 0/100 | 1.97 |
| SMR2 | 0.43 | 0.22 | 0.00 | 0.35 | 2.5 | 0.54 | 4.2 | 0/100 | 1.94 |
| SMF2 | 0.43 | 0.22 | 0.00 | 0.35 | 2.5 | 0.54 | 4.2 | 0/100 | 1.94 |
| SPK2 | 0.43 | 0.22 | 0.00 | 0.35 | 2.5 | 0.54 | 4.2 | 0/100 | 1.94 |
| N1S0 | 0.45 | 0.22 | 0.03 | 0.30 | 0 | 0.50 | 8.0 | 10/90 | 1.99 |
| N1SMR2 | 0.45 | 0.22 | 0.03 | 0.30 | 2.5 | 0.50 | 8.0 | 10/90 | 1.95 |
| N1SMF2 | 0.45 | 0.22 | 0.03 | 0.30 | 2.5 | 0.50 | 8.0 | 10/90 | 1.95 |
| N1SPK2 | 0.45 | 0.22 | 0.03 | 0.30 | 2.5 | 0.50 | 8.0 | 10/90 | 1.95 |
| N2S0 | 0.45 | 0.22 | 0.06 | 0.27 | 0 | 0.50 | 11.9 | 20/80 | 1.98 |
| N2SMR2 | 0.45 | 0.22 | 0.06 | 0.27 | 2.5 | 0.50 | 11.9 | 20/80 | 1.95 |
| N2SMF2 | 0.45 | 0.22 | 0.06 | 0.27 | 2.5 | 0.50 | 11.9 | 20/80 | 1.95 |
| N2SPK2 | 0.45 | 0.22 | 0.06 | 0.27 | 2.5 | 0.50 | 11.9 | 20/80 | 1.95 |


Figure 3.15. The process of preparation of SGP a) preparing the material for each mixture, b) and c) blending and mixing the materials, d) preparation of the chemical admixture, e) casting mixture into the prism and cube molds.

In the study, the most important issue is preparing the activator solution, because 3 different solutions using $Na_2SiO_3$ and 10M NaOH were used in different percentages. In preparing the solution, firstly NaOH in 10M concentration was prepared with water and then quickly mixed with $Na_2SiO_{3(aq)}$ (Ms:1/2). Thus, the temperature of the total solution made of $Na_2SiO_{3(aq)}$ and the 10M NaOH increased to roughly 50 $^oC$ because of 10M NaOH solution. in 10M concentration was replaced by $Na_2SiO_3$ in percentages of 10%, and 20% in the experimental studies. In the first stage NaOH were used at 0% and 10% replacement ratios, while 0%, 10% and 20% replacement ratios were used in the second stage of the study.

### 3.1.1. Test Methods

#### 3.1.1.1. Fresh State Tests of SGPs

After preparing the SGPs, it was subjected to many laboratory tests as follows: The Marsh funnel test was carried out according to ASTM D6910-04 [71]. In the test, fresh-state SGPs were placed into the Marsh funnel, and in the meantime orifice of

the Marsh funnel was covered by a finger as shown in Figure 3.14b. The funnel was carried over a graduated cup, and then the orifice was opened, and SGPs flow down while chronometry (timer) was beginning instantly. The time required to fill the graduated cup with SGP was measured in minutes, which is named funnel time. During the March funnel test performing, and flow table test was conducted according to ASTM C230 [114]. Firstly, the flow table was cleaned and dried out, and then the SGP was placed into a conical mold after being placed and centered on the flow table as shown in Figure 3.12d. The conical mold dimensions are 70 mm, 100 mm, and 50 mm for the diameter of the top, the diameter of the bottom and, the height of the mold respectively. Each SGP was placed in the conical mold and the mold lifted to flow SGP. By using a tape measure the diameter of the paste was measured along two lines, the diameters values were recorded and calculated as average values. Finally, the setting time of SGPs was measured based on ASTM C191 [115], where penetration tests every 15 minutes were performed on the SGPs to determine the final hardening time of SGPs.


Figure 3.16. March funnel and flow table tests.

### 3.1.1.2. Hardened State Tests of SGP

Generally, flexural strength is considered one of the most significant mechanical properties of materials, which displays the prismatic specimen's ability to resist bending failure. The prism specimens with size 40x40x160 mm were prepared and tested according to ASTM C 348-18 [116]. Three specimens were adopted for the flexural strength test to calculate average values. The tests were performed at 7, 28, and 90 days, as shown in Figure 3.17. Specific equations were followed according to ASTM C 348 to calculate the flexural strength values of SGPs:

$$\sigma_e = \frac{3PL}{2bd^2} \tag{3.1}$$

Where: $\boldsymbol{\sigma_e}$**:** Flexural strength (MPa)

**L:** Distance between the two carrying points of the sample.
**P:** The ultimate load read at the moment of breaking the sample.
**b:** Cross-section short side length.
**d:** Cross-section long side length.

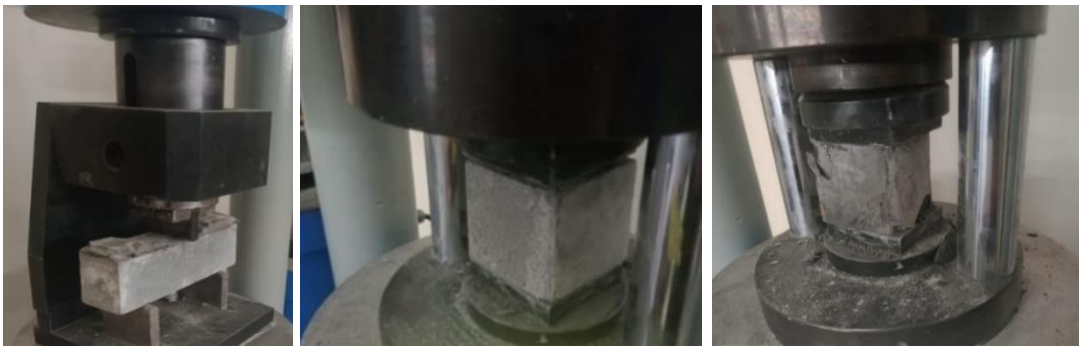

Figure 3.17. Flexural and compressive strength test equipment for testing of SGPs.

Cube specimens with dimensions 50x50x50 mm at 7, 28, and 90 days were performed to determine the compressive strengths of SGPs as shown in Figure 3.17. Three specimens were used for the compressive strength test according to ASTM C 109 [117]. The equation shown below was used to calculate compressive strength:

$$fm = \frac{P}{A} \quad (3.2)$$

Where; $f_m$ = Compressive strength MPa.
P = Total maximum load, N
A = area of loaded surface, $mm^2$.

Water absorption test was carried out as described in ASTM C20 [118]. A water absorption test was conducted for second stage SGPs after 28 days of production. The test procedure began with the specimens submerged in water for 24 h. The mass of saturated specimens is weighed ($M_1$) and their weight in water is also weighed ($M_2$). After that, the saturated specimens were put into an oven to get dry conditions specimens for at least 24 h at 105 °C. The weight of dried specimens was measured ($M_0$) after being taken out from the oven. The equations were given below to calculate the apparent porosity, specific gravity, and water absorption of SGPs conforming to ASTM C20.

$$W\ (\%) = \frac{M1-M0}{M0} \text{ x } 100 \quad (3.3)$$

$$\delta = \frac{M0}{M0-M2} \quad (3.4)$$

$$Pg = \frac{W*M0}{M1-M2} \quad (3.5)$$

Where; W = Water absorption rate (%). Pg = Apparent porosity.
$\delta$ = Specific gravity. $M_0$ = Dry weight.
$M_1$ = Specimen weight in saturated surface dry condition.
$M_2$ = Specimen weight in water.

### 3.1.1.3. Microstructural Examinations

To determine the microstructural systems of the hardened AAPs, Scanning Electron Microscopy (SEM) and Energy Dispersive Spectroscopy (EDX) analysis were performed on the 28$^{th}$ day in Research Center of Karabuk University. Approximately

3 different regions on the hardened AAPs were inspected in each specimen. During all SEM observations, the same structures were observed in each AAP. However, in here, only one region is shown and analyzed. In the figures below 2 SEM images, one of them drawn by rectangular shape on the source SEM image is a 2.5X enlarged image from the source. In addition, EDX analyses as both graphical and elemental analyses from some important areas are given as well.

# PART 4

# RESULTS AND DISCUSSION

This chapter shows details belonging to the results and discussions of alkali-activated ETS ash/GGBFS-based geopolymer pastes containing different types of high-ranged SP. The aim of this study is to determine the effects of various SPs on the workability and mechanical characteristics of SGPs. Test results of the study findings and detailed discussions are presented in this section.

## 4.1. RESULTS AND DISCUSSIONS OF FIRST STAGE STUDY

### 4.1.1. Marsh Funnel and Flow Table Tests Results

In the first stage of the study, Marsh funnel time (seconds), flow spreading diameter (cm), and setting time (min) tests of fresh state SGPs were performed, and their results are given in Figure 4.1 and in Table 4.1. Figure 4.1. shows the correlation between March funnel time and flow diameter. So, there is a good correlation between March funnel time and flow diameter in second degree (polynomic) equation.

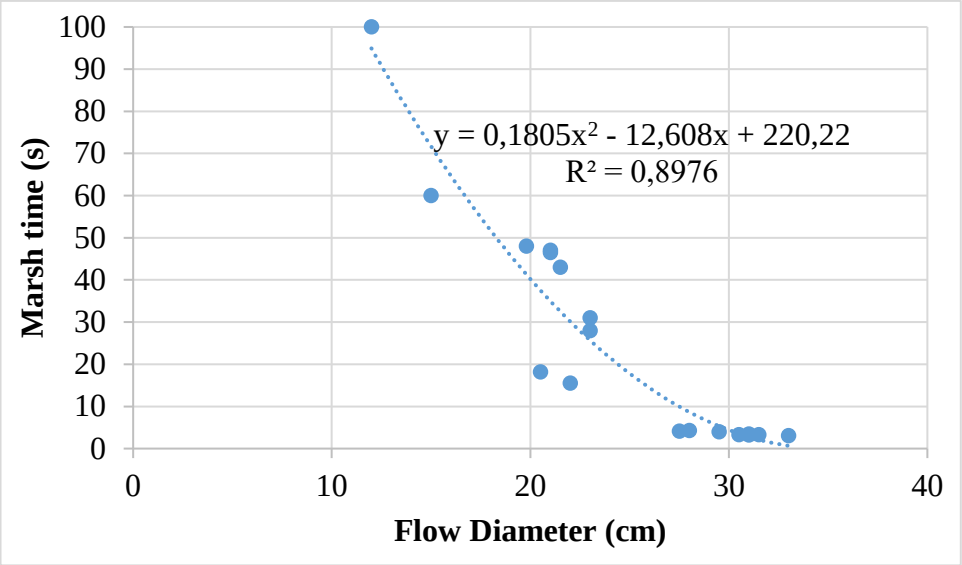


Figure 4.1. Correlation between Marsh Funnel time and flow diameter.

Table 4.1. Results of Fresh state tests of Geopolymer paste.

| Codes | NaOH (%) | Marsh funnel time (seconds) | Flow Diameter (cm) | Setting Time (min) | Codes | NaOH (%) | Marsh funnel time (min) | Flow Diameter (cm) | Setting Time (min) |
|---|---|---|---|---|---|---|---|---|---|
| **E0** | 0 | 47 | 21.0 | 180 | | | | | |
| **EMR5** | | 164 | 12.0 | 210 | | | | | |
| **S0** | | 16 | 22.0 | 225 | **NS0** | 10 | 3.07 | 33.0 | 110 |
| **SMR1** | | 18 | 20.5 | 150 | **NSMR1** | | 3.43 | 31.0 | 60 |
| **SMR2** | | 47 | 21.0 | 180 | **NSMR2** | | 3.23 | 31.0 | 90 |
| **SMR5** | | - | - | - | **NSMR5** | | - | - | - |
| **SMF1** | | 28 | 23.0 | 500 | **NSMF1** | | 3.30 | 31.5 | 90 |
| **SMF2** | | 31 | 23.0 | 150 | **NSMF2** | | 4.15 | 27.5 | 70 |
| **SMF5** | | - | - | - | **NSMF5** | | - | - | - |
| **SPK1** | | 48 | 19.8 | 700 | **NSPK1** | | 4.00 | 29.5 | 120 |
| **SPK2** | | 43 | 21.5 | 120 | **NSPK2** | | 3.30 | 30.5 | 90 |
| **SPK5** | | 60 | 15.0 | 75 | **NSPK5** | | 4.30 | 28.0 | 90 |

Since SMR5, SMF5, NSMR5, and NSMF5 did not show flow capability in the Marsh Funnel test, although the solution/powder ratio was 1.2, the abovementioned experiments didn't add to Table 4.1.

According to the results of fresh SGPs given in Table 4.1:

As the MEROS ash ratio in the SGPs increases, the marsh funnel time increases, especially for mixtures without any NaOH. However, there is no noticeable effect was observed of the addition of the MEROS ash on flow diameter as in mixtures SMR1 and SMR2. Meanwhile, by addition of 2.5% of MEROS ash into the mixture caused an increment in the setting time by 16% for mixture SMR2 without NaOH and 34% for NSMR2 with 10% NaOH.

The effect of SMF addition on Marsh funnel time was more evident in mixtures with 10% NaOH (NSMF1, and NSMF2). The marsh funnel time of NSMF2 is 45 min more than NSMF1. On the SGPs without NaOH, it is observed that the SMF doesn't significant effect on flow diameters. As the ratio of SMF increased, the setting time decreased. The setting time of NSMF1 and NSMF2 decreased by 70%, and 23% as compared with SMF1 and SMF2, respectively.

As the PCE ratio in the SGPs without NaOH increased, and the flow diameter decreased but the Marsh funnel time increased. However, in the SGPs with NaOH, PCE admixture is not significant effect on the marsh funnel time and flowability. PCE admixture reduced the setting time in all SGPs at different ratios. The marsh time of mixture SPK5 increased by 20% in comparison with SPK2. The flow diameter of the mixture SPK2 increased by 8% according to SPK5.

According to Marsh Funnel test results, NaOH caused a possible effect on the flowability of all mixtures significantly, because of the surfactant structure of NaOH [119]. For instance, the viscosity for the Marsh Funnel of NS0 is lower by approximately 500% than S0. There is no significant effect in flowability, when MEROS ash, MF, and PK were added to all SGPs. However, the NaOH effect on the flowability is more effective than SP admixtures.

According to the flow table test results, NaOH caused an increment in the flow diameter in all mixtures. For example, the diameter increased by 27 % for the

mixture NSMF1 compared to the SMF1. The highest value was observed as 31.5 cm on the NSMF1 mixture.

According to setting time results, except SPK5 specimen, NaOH decreased the setting time in all mixtures. For example, the setting time decreased by 83 % for mixture NSPK1 as compared with SPK1, except for mixture NSPK5 the setting time decreased significantly as the concentration of NaOH increased in the SGPs.

### 4.1.2. Results and Discussions of Flexural and Compressive Strength Tests

The flexural and compressive strengths test results of the study are given in Table 4.2. Given results in Table 4.2 are obtained from at least 3 specimens, and the average values were calculated and shown in Table 4.2 for each SGP.

Table 4.2. The mechanical properties of SGPs.

| **Code** | **N** | **Average Unit weights (g/cm$^3$) (Day)** | | | **Average Compressive Strength (MPa) (Day)** | | | **Average Flexural Strength (MPa) (Day)** | | | **NaOH (%)** |
|---|---|---|---|---|---|---|---|---|---|---|---|
| | | **7** | **28** | **90** | **7** | **28** | **90** | **7** | **28** | **90** | |
| **E0** | 11 | 1.48 | 1.33 | 1.19 | 0 | 5.6 | 15.7 | 0 | 0 | 0 | 0 |
| **EMR5** | 3 | 1.49 | 1.36 | 1.23 | 0 | 4.05 | 12.6 | 0 | 3.9 | 4.3 | |
| **S0** | 6 | 1.43 | 1.32 | 1.00 | 0 | 5.78 | 17 | 0 | 3.45 | 4.4 | |
| **SMR1** | 12 | 1.53 | 1.24 | 1.24 | 0 | 10.8 | 15.2 | 0 | 0 | 0 | |
| **SMR2** | 6 | 1.46 | 1.35 | 1.22 | 0 | 4.25 | 18 | 0 | 4.3 | 5.3 | |
| **SMF1** | 6 | 1.45 | 1.27 | 1.19 | 0 | 6.0 | 13.3 | 0 | 4.4 | 7.5 | |
| **SMF2** | 6 | 1.35 | 1.22 | 1.12 | 0.45 | 4.08 | 12.5 | 2.8 | 3.65 | 5.6 | |
| **SPK1** | 6 | 1.57 | 1.34 | 1.11 | 0 | 8.55 | 16.2 | 0 | 4.35 | 5.9 | |
| **SPK2** | 6 | 1.47 | 1.30 | 1.24 | 1.1 | 8.25 | 16.9 | 3 | 3 | 5.6 | |
| **SPK5** | 3 | 1.35 | 1.31 | 1.19 | 0 | 5.6 | 12.4 | 0 | 5 | 5.2 | |
| **NS0** | 3 | 1.51 | 1.40 | 1.32 | 11.8 | 11.2 | 13.5 | 6.4 | 4.8 | 7.2 | 10 |
| **NSMR1** | 3 | 1.49 | 1.36 | 1.32 | 8.23 | 10.8 | 12.4 | 5.4 | 4.8 | 5.3 | |
| **NSMR2** | 3 | 1.48 | 1.39 | 1.35 | 12.08 | 10.55 | 11.9 | 4.7 | 3.6 | 5.7 | |
| **NSMF1** | 3 | 1.44 | 1.29 | 1.30 | 6.33 | 9.4 | 11.5 | 3.8 | 3.9 | 4.9 | |
| **NSMF2** | 3 | 1.30 | 1.23 | 1.23 | 4.63 | 9.35 | 14.9 | 5 | 0 | 6.1 | |
| **NSPK1** | 3 | 1.53 | 1.44 | 1.30 | 12.9 | 9.75 | 11.9 | 0 | 4.6 | 4.4 | |
| **NSPK2** | 3 | 1.44 | 1.34 | 1.25 | 3.2 | 4.1 | 9.8 | 0 | 0 | 4.1 | |
| **NSPK5** | 3 | 1.44 | 1.47 | - | 2.23 | 0 | 0 | 3.9 | 0 | 0 | |

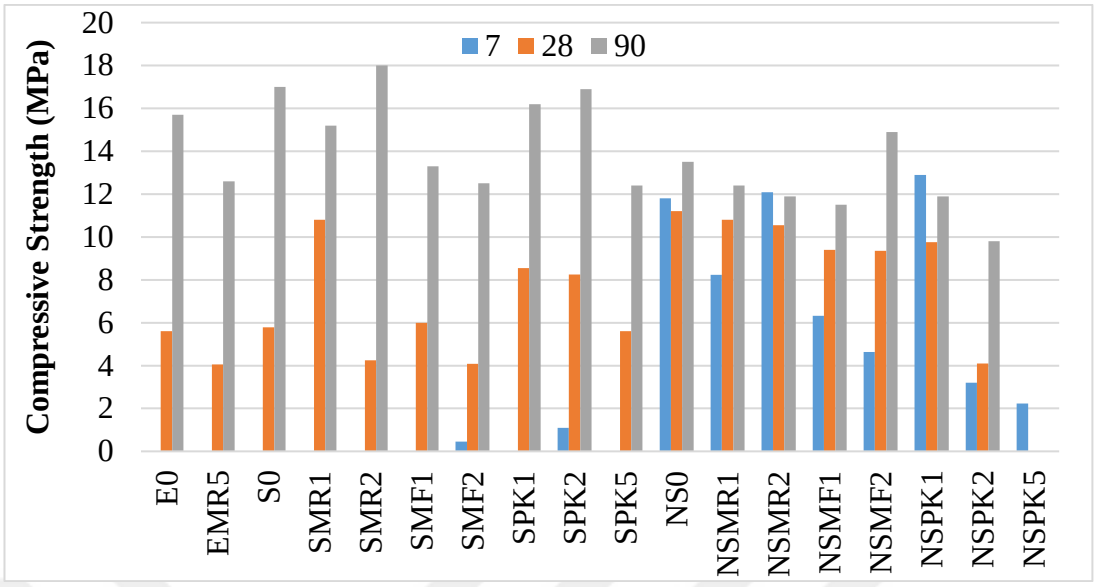


Figure 4.2. Compressive strength of SGPs without NaOH.

According to the results of compressive strengths given in Figure 4.2:

It was observed that compressive strength increased as NaOH concentration increased, especially at early ages. The compressive strength of the NSMF2 mixture increased by 90% compared with SMF2 because of NaOH. The compressive strength of SGPs increased significantly at 28 and 90 days. 28$^{th}$ and 90$^{th}$ day of the SPK2, increased by 87% and 93% compared to the 7$^{th}$ day compressive strengths, respectively.

The compressive strength of S0 is higher than 7.6% compared to E0. MEROS ash and NaOH improved the compressive strength of some SGPs. The addition of 1% MEROS ash increased compressive strength by 47% compared to S0 at 28 days. SMF admixture decreased the compressive strength of SGPs. However, the compressive strength of NSMF2's increased by 9.3% compared to the NS0 on the 90th day. PCE admixture increased mostly the compressive strength of SGPs. The addition of 1% PCE into the mixture increased the compressive strength by almost 32%.

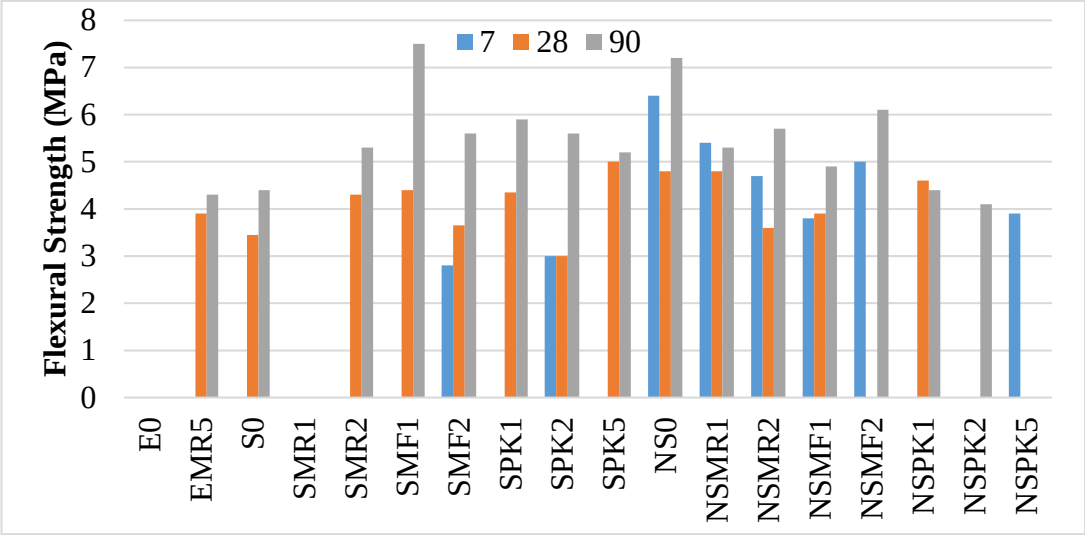


Figure 4.3. Mechanical properties of SGPs with NaOH.

According to the results of flexural strengths given in Figure 4.3:

10M NaOH addition to the SGPs caused an increase significantly in flexural strengths, especially in the early period. For example, the flexural strength of NS0 at 7 days was 6.4 MPa higher than S0.

The flexural strength increased with the age of SGPs. The flexural strength of some SGPs in the early period could not be determined because of higher solution/solid material ratios.

The MEROS ash to the mixture of SGPs without NaOH caused increasing in flexural strength, but the MEROS ash to the mixture of SGPs without NaOH caused decreasing in flexural strength. For example, the flexural strength of the mixture NSMR2 decreased by 25% as compared to NS0. Whereas there was a clear improvement in the flexural strength of specimens tested at 28 days for the mixture SMR0 by 19.8 % in comparison with S0. On the other hand, the SMF has the same effect as the MEROS ash. The flexural strength of the mixture NSMF1 decreased by 18.8% compared to the NS0, while the mixture SMF2 showed an increment in flexural strength by 5.5% versus the mixture S0. While PCE-type SP increased the flexural strength of the SGP mixtures without NaOH, the flexural strength of the

other SGP mixtures with NaOH decreased. The flexural strength of the NSPK2 mixture decreased by 39% in compared to the NS0 tested at 28 days of age.

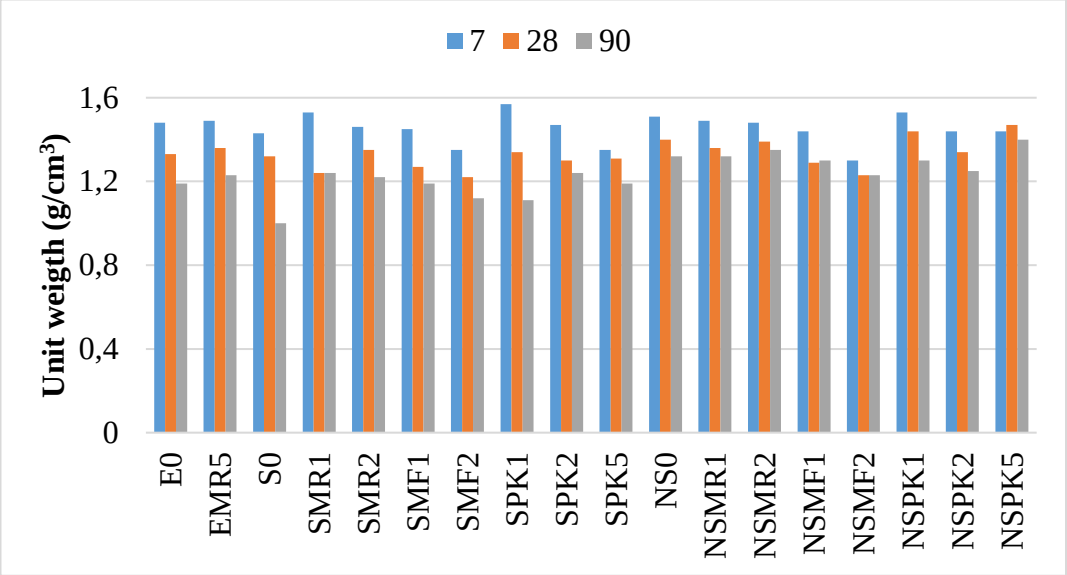


Figure 4.4. Diagram of average unit weights of SGPs.

From Figure 4.4 it was detected that:

The unit weight for SGP samples at 7 – 90 days ranges between 1.001 -1.569 g/cm3. It was detected that the unit weight decreased as the curing age increased, this is due to the evaporation of excess water in SGPs. For example, SGP unit weights decreased by 10.7% and 20% for samples tested at 28 and 90 days as compared with that tested at 7 days. SP and MEROS ash don't affect unit weight significantly.

## 4.2. THE RESULTS AND DISCUSSIONS OF THE SECOND PHASE EXPERIMENTS

### 4.2.1. Compressive Strength Tests Results and Discussions

As a second step, mixtures were prepared with different ratios of sodium hydroxide by (0, 10, and 20) % and with a constant water reducer (MEROS ash, SMF and PCEs) in 2.5% ratio. The specimens were cured in a furnace at 80 °C for 3 hours and mechanically tested at 2 and 28 days as mentioned in Table 4.3.

Table 4.3. Compressive Strength of SGPs.

| Codes | Average Unit weights ($g/cm^3$) | | Average Compressive strength (MPa) | | NaOH (%) |
|---|---|---|---|---|---|
| | 2 days | 28 days | 2 days | 28 days | |
| S | 1.82 | 1.57 | 4.4 | 18.4 | 0 |
| SMR | 1.53 | 1.56 | 2.8 | 18.53 | |
| SMF | 1.69 | 1.52 | 2.55 | 15 | |
| SPK | 1.55 | 1.45 | 2.9 | 9.4 | |
| NaS | 1.77 | 1.67 | 26.75 | 36.95 | 10 |
| NaSMR | 1.84 | 1.67 | 22.1 | 30.55 | |
| NaSMF | 1.77 | 1.65 | 17.35 | 27.25 | |
| NaSPK | 1.68 | 1.59 | 15.4 | 23.55 | |
| NbS | 1.81 | 1.76 | 27.4 | 41.75 | 20 |
| NbSMR | 1.82 | 1.52 | 19.4 | 33.3 | |
| NbSMF | 1.71 | 1.39 | 17.7 | 20.25 | |
| NbSPK | 1.72 | 1.26 | 17.2 | 12.5 | |

Table 4.3 and Figure 4.5 are discussed below:

According to the compressive strength test results, the maximum compressive strengths of SGPs on 2nd day are obtained by 4.4 MPa, 26.75 MPa, and 27.4 MPa for S, NaS, and NbS, respectively. And the maximum compressive strengths of SGPs on 28nd day are obtained by 18.53 MPa, 36.95 MPa, and 41.75 MPa for S0, NS1, and N2S, respectively. Hence, as the NaOH ratio increased in SGPs, the compressive strength of SGPs increased dramatically. In these results, 10% and 20% NaOH in the SGPs cause increasing compressive strength by approximately 608% and 623% on the $2^{nd}$ day respectively. Moreover, on the 28th day, the compressive strength of SGPs with 10% and 20% NaOH increased by approximately 199% and 225% respectively.

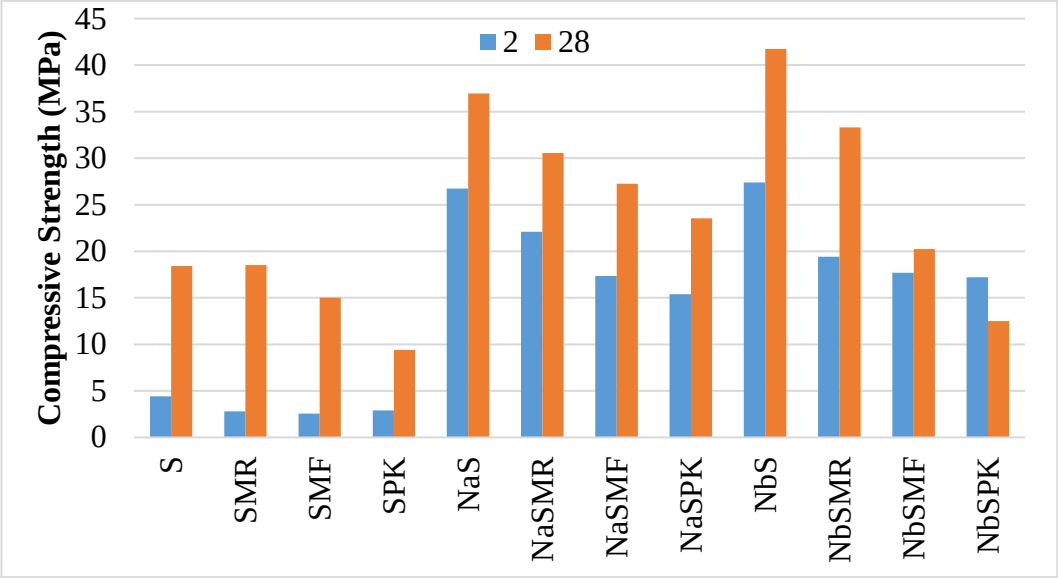


Figure 4.5. Compressive strength of SGPs.

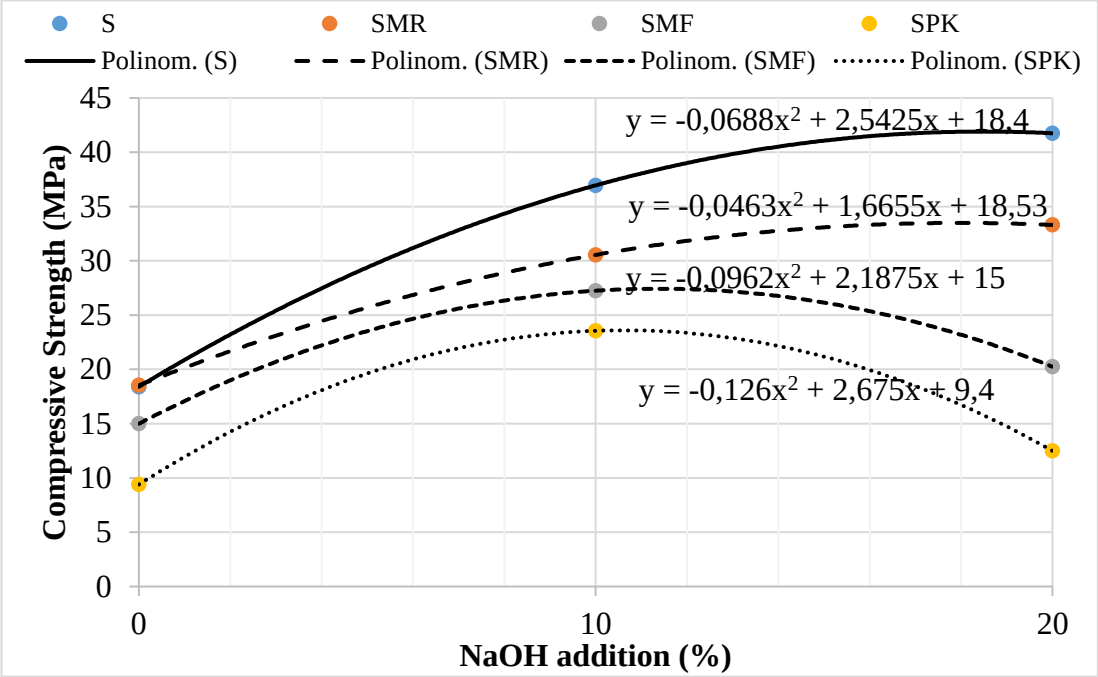


Figure 4.6. Compressive strength of SGPs for 28th day age.

On the other hand, all SPs caused decreasing in the compressive strength of SGPs in different ratios. However, MEROS ash in a little increased compressive strength on the 28th day differently from the others. The compressive strength had affected negatively by MEROS ash, SMF, and PCE admixtures from minimum to maximum respectively.

According to Figure 4.6., while the compressive strengths of reference and MEROS-added SGPs increased by NaOH addition, the compressive strengths of SMF and PCE-added SGPs decreased by NaOH addition, especially after %10. Consequently, when NaOH was added to the SGPs, MEROS ash, SMF, and PCE-based admixtures decreased compressive strength dramatically. However, admixtures in the SGPs affected the compressive strengths of SGPs without NaOH slightly. Moreover, as NaOH increase in the SGP, the admixtures' effect on the compressive strength increases negatively.

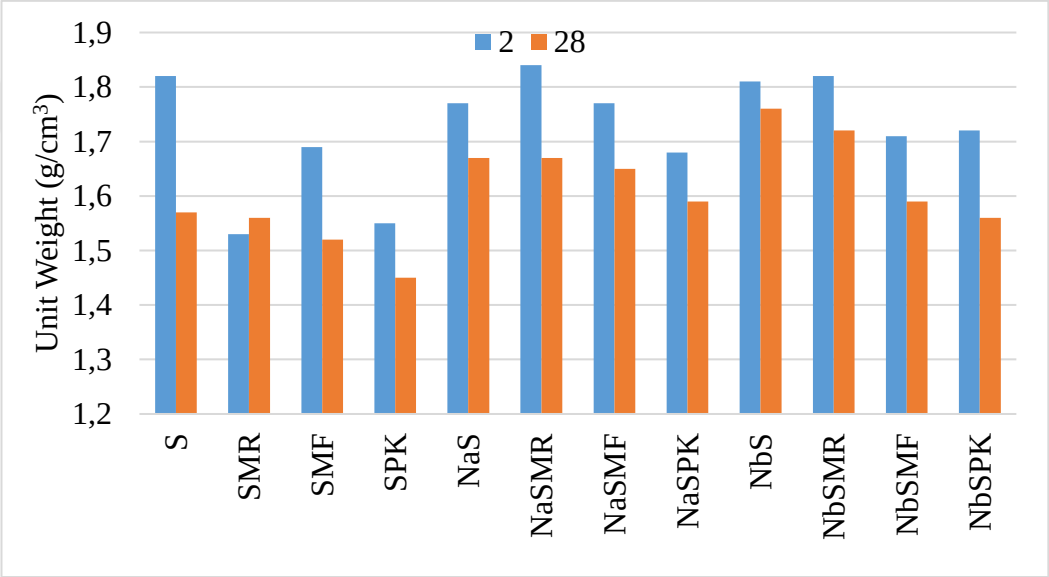


Figure 4.7. Unit weight of SGPs.

According to Figure 4.7, the unit weight was varied between 1.46 – 1.75 g/cm3 for SGP samples tested at 28 days. The testing age also plays an important role in the reduction of unit weight. For example, the unit weight decreased by 10% for mixture NSMR2 tested at age 28 days as compared to 2 days.

### 4.2.2. Water Absorption

Results for apparent porosity (in %) and water absorption (in %) for SGPs on 28th day are shown in Table 4.4.

Table 4.4. Results of water absorption test.

| Code | Dry apparent specific gravity | Water Absorption (weight) | Apparent porosity (%) | NaOH (%) |
|---|---|---|---|---|
| S | 1.27 | 18.90 | 24.08 | 0 |
| SMR | No water resistant | | | |
| SMF | 1.30 | 16.77 | 21.84 | |
| SPK | 1.25 | 19.97 | 24.88 | |
| NaS | 1.42 | 16.39 | 23.31 | 10 |
| NaSMR | 1.48 | 16.72 | 24.69 | |
| NaSMF | 1.38 | 13.17 | 18.17 | |
| NaSPK | 1.35 | 13.44 | 18.11 | |
| NbS | 1.47 | 15.67 | 23.06 | 20 |
| NbSMR | 1.44 | 15.94 | 23.01 | |
| NbSMF | 1.31 | 13.91 | 18.28 | |
| NbSPK | 1.35 | 14.39 | 19.37 | |

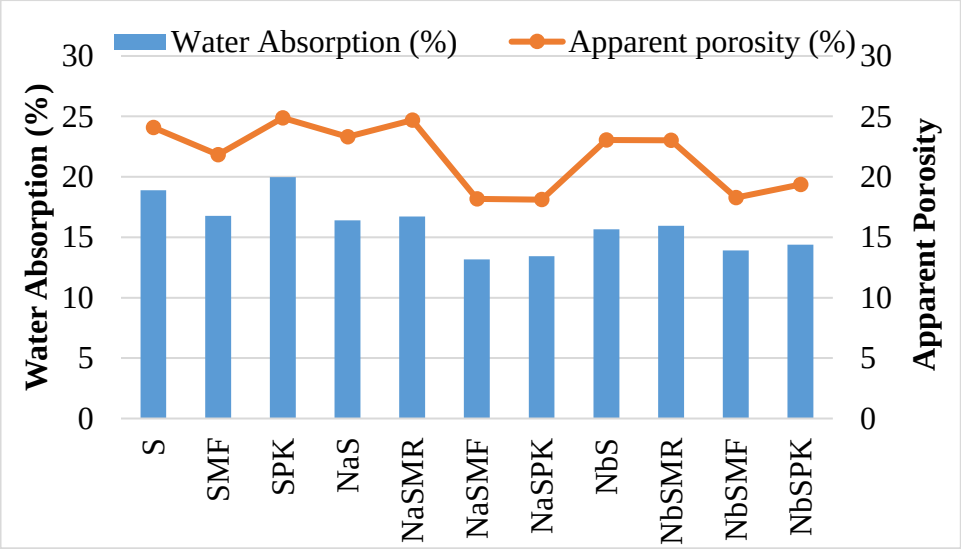


Figure 4.8. The relation between water absorption and apparent porosity of specimens after 28 days of production.

The results of water absorption and apparent porosity are discussed below according to Figure 4.8:

According to Figure 4.8, NaOH used in SGPs caused decreasing water absorption dramatically. The average absorption was 13.17%, 13.44%, 13.91%, and 14.39% for mixtures NSMF2, NSPK2, NSMF3, and NSPK3 respectively. The percentage of

porosity decreased by 18.17%, 18.11%, 18.28%, and 19.37%, respectively, for the samples NSMF2, NSPK2, NSMF3, and NSPK3 evaluated under identical conditions. Adding 10% NaOH and 2.5% water reducer, in particular Melamine formaldehyde and Polycarboxylic ether-based superplasticizer, caused the sample structure to become denser, tougher, and enhanced crystallinity.

The NaOH concentration had a significant role in improving the apparent porosity and minimizing water absorption. As NaOH concentration rose from 0% to 10%, NSPK3's water absorption decreased by 32%. When NaOH concentration reached 20%, SGPs' water absorption percentage rose again. NSPK3's water absorption rate rose by 7% when NaOH concentration reached 20%.

### 4.2.3. Microstructural Examinations

To determine the microstructural systems of the hardened AAPs, Scanning Electron Microscopy (SEM) and Energy Dispersive Spectroscopy (EDX) analysis were performed on the 28$^{th}$ day. Approximately 3 different regions on the hardened AAPs were inspected in each specimen. During all SEM observations, the same structures were observed in each AAP. However, in here, only one region is shown and analyzed. In the figures below 2 SEM images, one of them drawn by rectangular shape on the source SEM image is a 2.5X enlarged image from the source. In addition, EDX analyses as both graphical and elemental analyses from some important areas are given as well. SEM and EDX analyses of YMR0 are shown in Figure 4.9. The rectangular line in Figure 4.9a-c is magnified at 2.5X and shown in Figure 4.9b-d. EDX analyses from 3 areas are shown in Figure 4.9 and the elemental mass of regions is shown in the Table given in Figure 4.9. According to the SEM images, some unreacted GGBFS and ETS on some dusting areas can be seen above the geopolymeric forms. The well-structured region can be seen in Figure 4.9a-b, in here good developed geopolymeric forms can be observed apparently. Moreover, following Figure 4.9a, particles bigger than 20 microns were not dissolved and reacted in an activated solution. Hence, these particles work like aggregates in the composite.

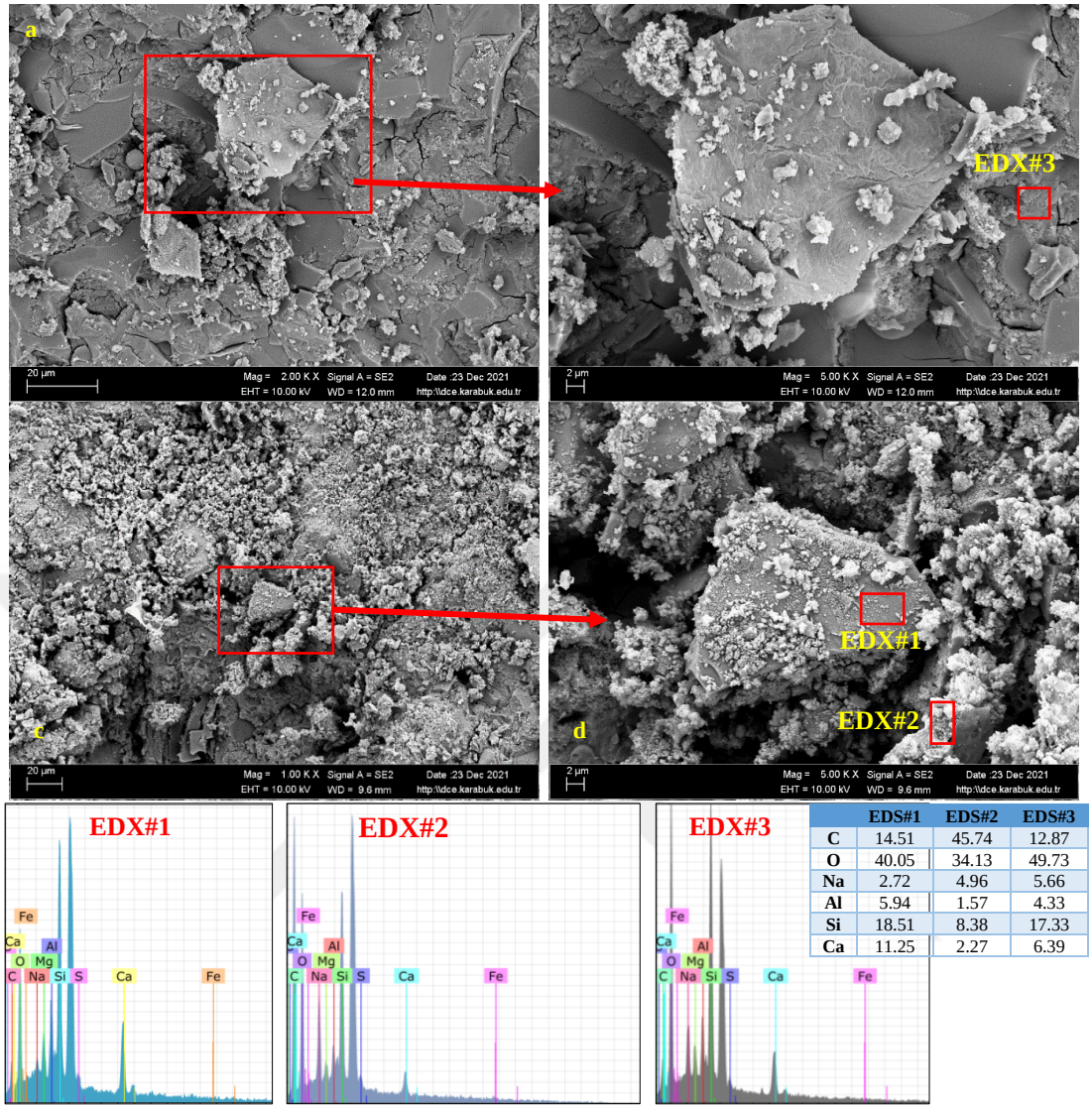


| | EDS#1 | EDS#2 | EDS#3 |
|---|---|---|---|
| C | 14.51 | 45.74 | 12.87 |
| O | 40.05 | 34.13 | 49.73 |
| Na | 2.72 | 4.96 | 5.66 |
| Al | 5.94 | 1.57 | 4.33 |
| Si | 18.51 | 8.38 | 17.33 |
| Ca | 11.25 | 2.27 | 6.39 |

Figure 4.9. SEM and EDX analyses of Reference paste.

According to EDX#1, these particles are akin to GGBFS because of their elemental structure and sharp geometry. In EDS#2, carbonated particles are observed. In EDS#3, N-(C)-A-S-H type geopolymeric forms between the unreacted particles are detected. Moreover, Si/Al ratio in EDS#3 is calculated as roughly 4 and Al/Na. In detailed looks, shrinkage cracks and weakness Interface Transition Zone (ITZ) lines can be seen clearly in Figure 4.9a-b. However, well-formed ITZ in some areas is also observed in the figures as well. The average compressive strength of Ra composite pastes was obtained as 18 MPa on the 28$^{th}$ day, and this is also the average value among the other composite pastes. Thus, the reason for relatively lower compressive strength can be unreacted particles, weakness ITZ and cracks due to the shrinkage in

geopolymeric forms, and so, continuity of structure was limited because of these, and compressive strength obtained lower.

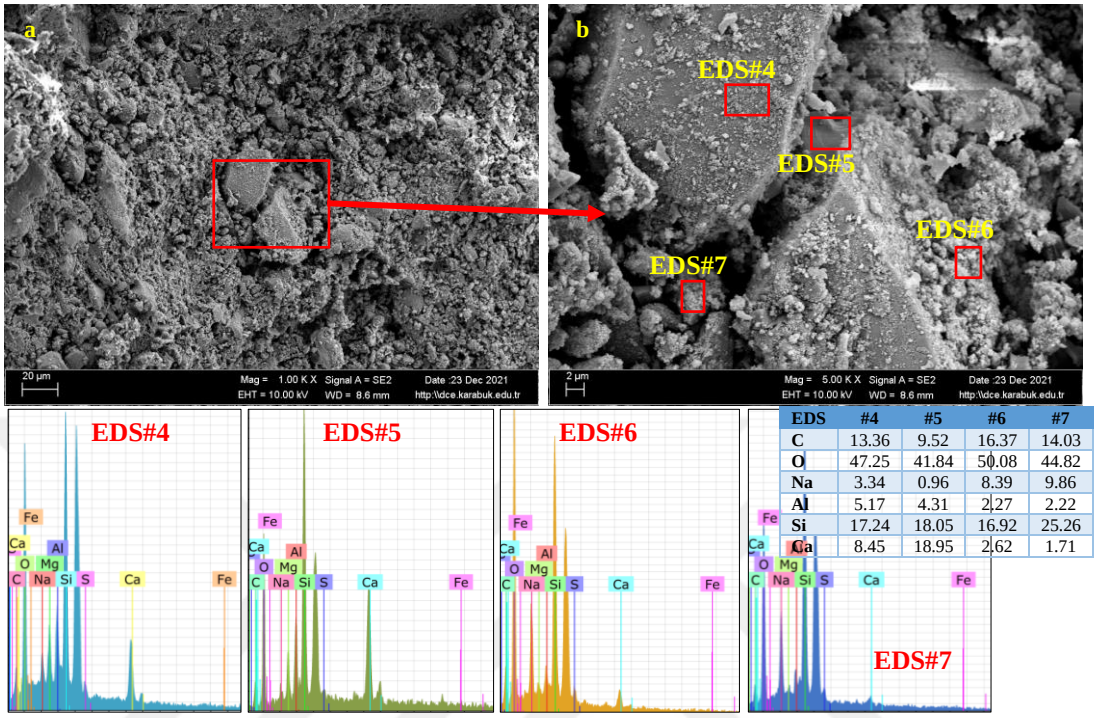


| EDS | #4 | #5 | #6 | #7 |
|---|---|---|---|---|
| C | 13.36 | 9.52 | 16.37 | 14.03 |
| O | 47.25 | 41.84 | 50.08 | 44.82 |
| Na | 3.34 | 0.96 | 8.39 | 9.86 |
| Al | 5.17 | 4.31 | 2.27 | 2.22 |
| Si | 17.24 | 18.05 | 16.92 | 25.26 |
| Ca | 8.45 | 18.95 | 2.62 | 1.71 |

Figure 4.10. SEM and EDX analyses of SMR paste.

Figure 4.10 shows the SEM images and EDS analyses of MEROS ash added geopolymer paste with 5% (by weight) MEROS ash. During the SEM observation, lots of unreacted ETS ash and GGBFS powder were obtained. Especially, particles mostly bigger than 20 microns were not participated in the activation progress like on the Reference AAC. According to the EDX analyses, the most of particles are unreacted GGBFS as can be seen on EDS#4 and EDS#5. EDS#6 and EDS #7 are weak-formed geopolymeric structures because N-A-S-H was detected on their body according to the element table in Figure 4.10. In here, Si/Al ratio is calculated at almost 8 and 12 for EDS#6 and #7 respectively, and Na/Al ratio is calculated as between 4-5. Moreover, carbonated forms are detected as well. Hence, the compressive strength of SMF AAC is approximately 18 MPa on the 28$^{th}$ day. Moreover, according to the EDX analyses, sulfur-bonded structures like $SO_4$ or $SO_3$ coming from MEROS ash are detected on the surface of the SMF paste. Even though lots of powdered regions were observed on SEM images of the SMF paste, its

compressive strength of its akin to the reference paste. Thus, it can be mentioned that the sulfur-based forms effect positively on strength of the SMF paste.

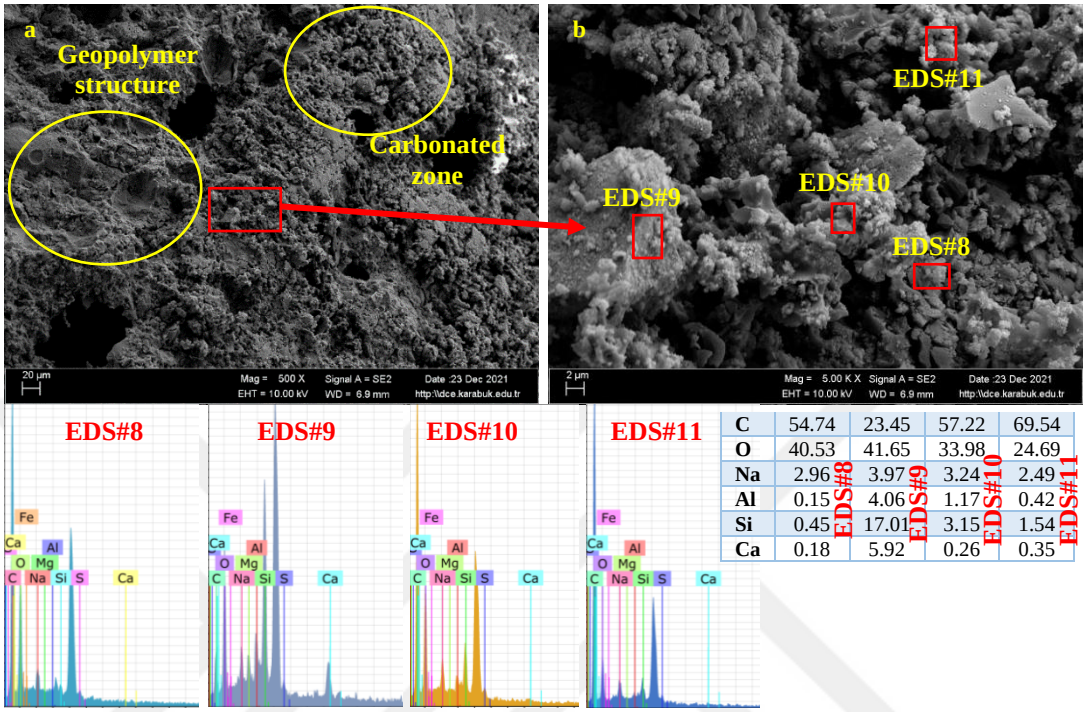


| | EDS#8 | EDS#9 | EDS#10 | EDS#11 |
|---|---|---|---|---|
| C | 54.74 | 23.45 | 57.22 | 69.54 |
| O | 40.53 | 41.65 | 33.98 | 24.69 |
| Na | 2.96 | 3.97 | 3.24 | 2.49 |
| Al | 0.15 | 4.06 | 1.17 | 0.42 |
| Si | 0.45 | 17.01 | 3.15 | 1.54 |
| Ca | 0.18 | 5.92 | 0.26 | 0.35 |

Figure 4.11. SEM and EDX analyses of SMF paste.

In Figure 4.11, SEM images and EDS analyses of melamine formaldehyde-based SP-added geopolymer paste are shown. The SEM image given in Figure 4.11a illustrates two different structures: geopolymer structures and carbonated particles. Carbonated structures are covered almost all of the surface. Regions of EDS#8, 10, and 11 areas are defined as carbonated structures. These are $Na_2CO_3$ forms coming from melamine formaldehyde or the effect of $Na_2O$; therefore, the compressive strength of the M3 pastes was obtained as 15 MPa.

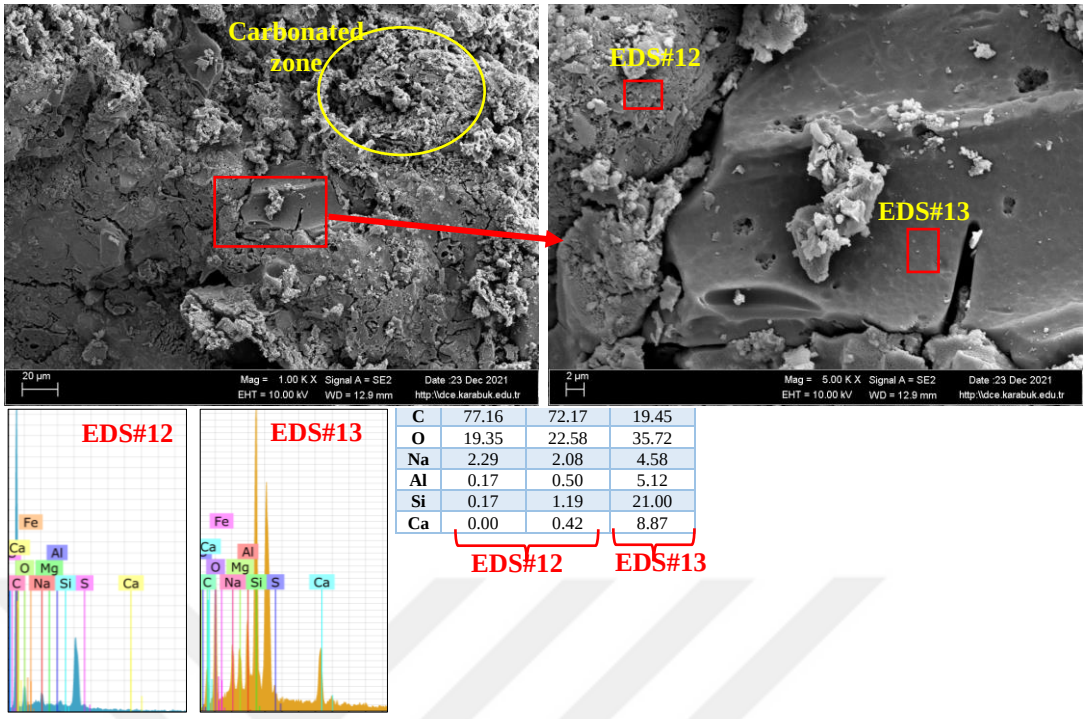


| | | | |
|---|---|---|---|
| **C** | 77.16 | 72.17 | 19.45 |
| **O** | 19.35 | 22.58 | 35.72 |
| **Na** | 2.29 | 2.08 | 4.58 |
| **Al** | 0.17 | 0.50 | 5.12 |
| **Si** | 0.17 | 1.19 | 21.00 |
| **Ca** | 0.00 | 0.42 | 8.87 |
| | | **EDS#12** | **EDS#13** |

Figure 4.12. SEM and EDX analyses of SPK paste.

Figure 4.12. illustrates the SEM images and EDS analyses of polycarboxylate ether-based SP-added geopolymer paste. As it is similar to the SPK paste, carbonated and geopolymeric structures on the surface of the SPK paste can be seen clearly. EDS analyses give some details about elemental analysis and depict some of the regions of carbonated and geopolymeric structures. EDS#12 depicts a carbonate form, but EDS#13 shows the GGBFS. So, as it mentioned above, the particles higher than 20 microns did not join in geopolymeric reactions.

Figure 4.13 shows the SEM and EDS analyses of the SGP with MEROS ash and %10 NaOH specimen. On the image, unreacted GGBFS and ETS ash particles were observed as especially bigger than 20-micron particles. These particles exist in the pastes like aggregates, and ITZ structures are mostly in the quite weak form. Cracks between particles and paste are obvious. EDS#14 and #15 shows the GGBFS and ETS ash particles respectively. However, EDS#16 shows a geopolymeric structure since this region has N-(C)-A-S-H like structure. In this specimen's SEM images, there are lots of well-formed structure were observed.

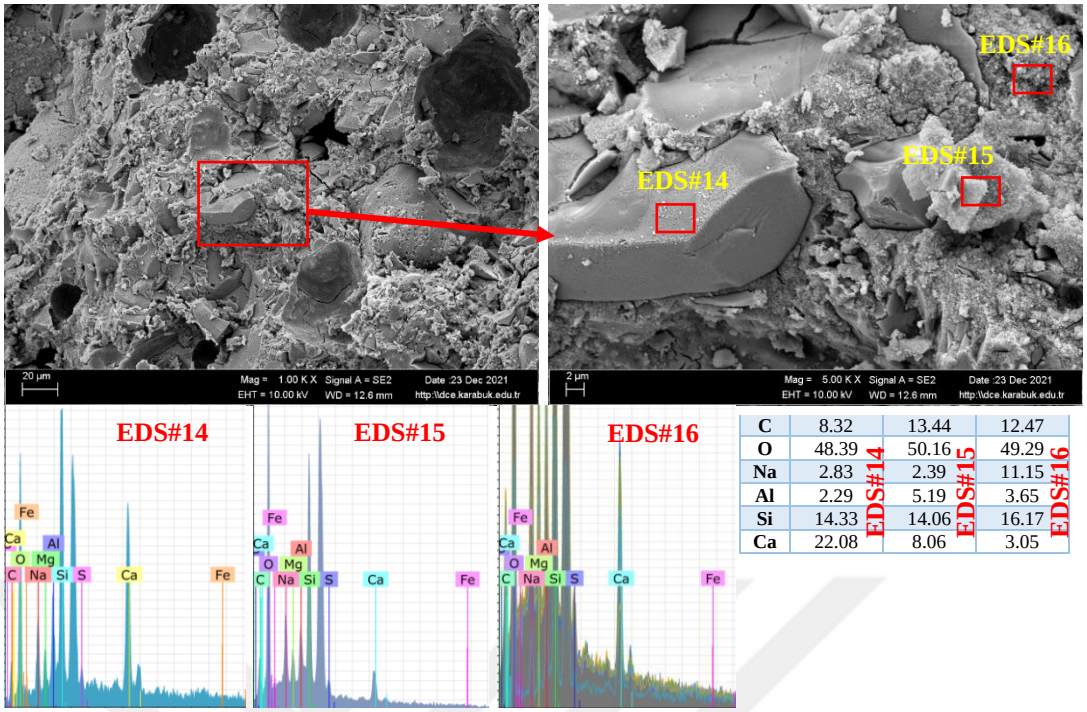


| | EDS#14 | EDS#15 | EDS#16 |
|---|---|---|---|
| C | 8.32 | 13.44 | 12.47 |
| O | 48.39 | 50.16 | 49.29 |
| Na | 2.83 | 2.39 | 11.15 |
| Al | 2.29 | 5.19 | 3.65 |
| Si | 14.33 | 14.06 | 16.17 |
| Ca | 22.08 | 8.06 | 3.05 |

Figure 4.13. SEM and EDX analyses of NaMR paste.

Figure 4.14 shows the XRD analyses of some SGPs. According to the analyses, all SGPs, except SMR, have amorph structure on their body, and zeolite forms mostly obtained. However, there are also calcite, quartz, and C-S-H structures. On some SGPs like NbSPK, ferritin phase is observed.

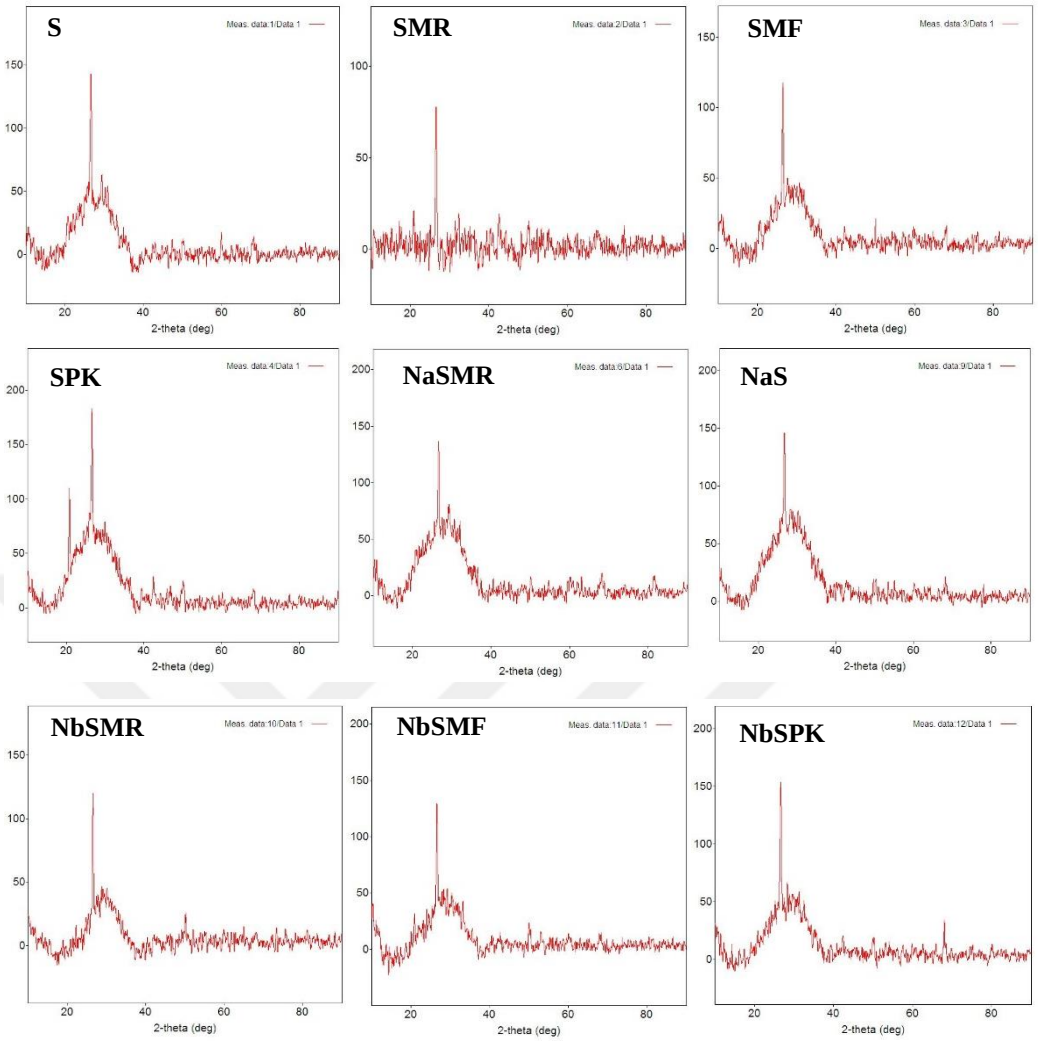


Figure 4.14. XRD analyses of SGPs.

Figure 4.15. The failure pattern of the cube sample prepared by the addition PCE.

Figure 4.15. represents the samples of N-YPK3 mixture with 10% 10M NaOH and 1% of PCE-based SP after being tested under compressive strength. On the images, there are differences in disruption types between specimens prepared with 0%

(YMR0), and 10 % (N1-YMR0). It is observed that the samples of the N1-YMR0 mixture possess good quality on the photos because of the NaOH effect to higher strength.

Figure 4.16. a) MEROS ash, b) PCEs, and c) SMF.

The Samples for mixture N-YPK3 that contains 1% PCE and 10% concentration of NaOH possess more rigid and smooth surfaces as compared with those containing MEROS ash (N-YMR1) and SMF (N-YMF3) respectively.

# PART 5

## CONCLUSION

The silica and alumina sources used in this research came from ETS ash and ground granulated blast furnace slag (GGBFS). For the alkali activators, a mixture of (100%, 90%, and 80%) sodium silicate (Na2SiO3) and (0%, 10% and 20%) sodium hydroxide (NaOH) was used. Workability, physical, and mechanical properties were determined with the usage of MEROS, PCEs, and SMF. Hardening time, flow table, and marsh funnel tests on every batch of the mix were performed. Moreover, on the 28th day of manufacturing, a water absorption test was performed on all mixed specimens. In addition, the SGPs were tested in physical and mechanical qualities at the $7^{th}$, $28^{th}$, and $90^{th}$ days into manufacture. The following conclusions may be derived based on the findings of this study:

- SGP mixtures with 10 % of 10 M of NaOH relatively possess high flowability.
- The existence of any water reducers (SMF, and PCEs) in the mixture did not satisfactory effect on the flowability.
- MEROS ash did not any effect on the strength of SGPs, regardless of setting time or workability. Its effect is zero for compressive strength, but when NaOH used in the mixture, MEROS ash effect positively.
- The presence of a high ratio of low calcium ETS ash in the mixture negatively affected the Marsh Funnel time but vice versa in the case of GGBFS utilized.
- The optimum funnel time was obtained in mixtures containing 10% of 10M NaOH, especially for mixtures with adding PCEs and SMF respectively.
- The highest flow diameter was observed for mixtures (N-SMR1), (N-SMR2), and (N-SMF2) with relatively close values, which were prepared with MEROS, and SMF respectively, and NaOH additive increases the effect of flowability.

- As the molarity of the concentration of NaOH increases the setting time decreases, this was observed in the mixture S and NS respectively.
- The existence of a water reducer (MEROS, SMF, and PCEs) in the mixture reduced the setting time.
- The setting time decreased as the ratio of slag increased in the mixture.
- The structure of specimens of SGPs becomes denser, harder, and improved crystallinity after the addition of water reducer (MEROS, SMF, and PCEs) in the mixture especially for those containing 10 % of NaOH.
- The compressive strength is directly proportional to the NaOH concentration and the existence of water reducers in the mixtures.
- The presence of GGBFS with a high ratio contributed to an increase at the early age strength, whereas SGP with an ETS ash/ slag ratio of 2:1 possess high compressive strength at late ages.
- The maximum flexural strength value was 7.5 MPa (for mix SMF1) prepared by 1 % of SMF with no NaOH used and tested at 90 days.
- The addition of 10% of NaOH to the mixture has a long-term effect on increasing the compressive strength of SGP, despite it doesn't have early age strength as compared with those consisting of 20 % of NaOH.

## REFERENCES


1. Roy, D. M., "Alkali-activated cements Opportunities and challenges", ***Cement And Concrete Research***, 29 (2): 249–254 (1999).

2. Aliabdo, A. A., Abd Elmoaty, A. E. M., and Salem, H. A., "Effect of cement addition, solution resting time and curing characteristics on fly ash based geopolymer concrete performance", ***Construction And Building Materials***, 123: 581–593 (2016).

3. Sakulich, A. R., "Reinforced geopolymer composites for enhanced material greenness and durability", ***Sustainable Cities And Society***, 1 (4): 195–210 (2011).

4. Abriyantoro, D., Dong, J., Hicks, C., and Singh, S. P., "A stochastic optimisation model for biomass outsourcing in the cement manufacturing industry with production planning constraints", ***Energy***, 169: 515–526 (2019).

5. Juenger, M. C. G., Winnefeld, F., Provis, J. L., and Ideker, J. H., "Advances in alternative cementitious binders", ***Cement And Concrete Research***, 41 (12): 1232–1243 (2011).

6. Unless, R., Act, P., Rose, W., If, T., Rose, W., "Advances in understanding alkali activated materials", (2015).

7. Pacheco-Torgal, Fernando, Castro Gomes, Joao, Jalali, S., "Alkali-activated binders: a review part I. Historical background, terminology, reaction mechanisms, and hydration products", ***Construction And Building Materials***, 1305–1314 (2008).

8. A. Mehta, R. S., "An overview of geopolymers derived from industrial byproducts, Constr", ***Build Mater***, 183–198 (2016).

9. S. Majhi, A. Mukherjee, A. F. S., "Thermal performance of an alkaliactivated paste for bonding fibre sheets with concrete", 43–53 (2019).

10. Ortega, E. A., Cheeseman, C., Knight, J., and Loizidou, M., "Properties of alkali-activated clinoptilolite", ***Cement And Concrete Research***, 1641–1646 (2000).

11. Ye, H. and Radlińska, A., "Quantitative Analysis of Phase Assemblage and Chemical Shrinkage of Alkali-Activated Slag", ***Journal Of Advanced Concrete Technology***, 245–260 (2016).

12. Yurt, Ü., "High performance cementless composites from alkali activated GGBFS", ***Construction And Building Materials***, 264: (2020).

13. Abhilash, P., Sashidhar, C., and Reddy, I. V. R., "Evaluation of performance of Geopolymer Concrete in acid environment", ***International Research Journal Of Engineering And Technology(IRJET)***, 4 (7): 1433–1438 (2017).

14. Balcikanli, M. and Ozbay, E., "Optimum design of alkali activated slag concretes for the low oxygen/chloride ion permeability and thermal conductivity", ***Composites Part B: Engineering***, 91: 243–256 (2016).

15. Aydın, S. and Baradan, B., "Effect of activator type and content on properties of alkali-activated slag mortars", ***Composites Part B: Engineering***, 57: 166–172 (2014).

16. Burgos-Montes, O., Palacios, M., Rivilla, P., & Puertas, F. (2012). Compatibility between superplasticizer admixtures and cements with mineral additions. ***Construction and Building Materials***, 31, 300-309.

17. Alsadey, S. (2012). Influence of superplasticizer on strength of concrete. I***nternational Journal of Research in Engineering and Technology***, 1(3), 164-166.

18. Tkaczewska, E. (2014). Effect of the superplasticizer type on the properties of the fly ash blended cement. C***onstruction and Building Materials***, 70, 388-393.

19. M. Akram Tahir, M. Sabir, A Study on durability of fly ash-cement mortars" ***30th Conference on our world in concrete & structures*** 2005.

20. Aparna, S., Sathyan, D., & Anand, K. B. (2018). Microstructural and rate of water absorption study on fly-ash incorporated cement mortar. ***Materials Today: Proceedings***, 5(11), 23692-23701.

21. Patel, Y. J. and Shah, N., "Enhancement of the properties of Ground Granulated Blast Furnace Slag based Self Compacting Geopolymer Concrete by incorporating Rice Husk Ash", ***Construction And Building Materials***, 171: 654–662 (2018).

22. Shahrajabian, F. and Behfarnia, K., "The effects of nano particles on freeze and thaw resistance of alkali-activated slag concrete", ***Construction And Building Materials***, 176: 172–178 (2018).

23. Fang, G., Ho, W. K., Tu, W., & Zhang, M. (2018). Workability and mechanical properties of alkali-activated fly ash-slag concrete cured at ambient temperature. ***Construction and Building Materials,*** 172, 476-487.

24. Nematollahi, B., & Sanjayan, J. (2014). Effect of different superplasticizers and activator combinations on workability and strength of fly ash based geopolymer. ***Materials & Design,*** 57, 667-672.

25. Taylor, M., Tam, C., and Gielen, D., "Energy Efficiency and CO 2 Emissions from the Global Cement Industry Energy Efficiency and CO 2 Emission Reduction Potentials and Policies in the Cement", (July 2014): 4–5 (2006).

26. Malhotra, V. M., "Introduction: Sustainable Development and Concrete Technology", ***Concrete International***, 24 (7): .

27. MCCAFFREY, R., "Climate Change and Cement Industry", ***Global Cement And Lime Magazine***, 15–19 (2002).

28. Mehta, B.Y.P.K. and Burrows, R.W., "Durable_Concrete_Structmehtaci 2001_178.Pdf" , (March): 57–63 (2001).

29. Puertas, F., Martínez-Ramírez, S., Alonso, S., and Vázquez, T., "Alkali-activated fly ash/slag cements: Strength behaviour and hydration products", ***Cement And Concrete Research***, 30 (10): 1625–1632 (2000).

30. Kuhl, H., "Slag cement and process of making the same", .

31. Purdon, A. O., "The action of alkalis on blast-furnace slag", ***Journal Of The Society Of Chemical Industry***, 59 (9): 191–202 (1940).

32. Glukhovsky, V., "Gruntosilikaty (Soil Silicates)", (1959).

33. Glukhovsky VD, Rostovskaja GS, R. G., "High strength slag alkaline cements", ***Proceedings Of The Seventh International Congress On The Chemistry Of Cement***, 164–8 (1980).

34. Davidovits, J., "Synthesis of new high temperature geo-polymers for reinforced plastics/composites", ***SPE PACTEC 79 Society Of Plastic Engineers***, (1979).

35. Li, C., Sun, H., and Li, L., "A review: The comparison between alkali-activated slag (Si + Ca) and metakaolin (Si + Al) cements", ***Cement And Concrete Research***, 40 (9): 1341–1349 (2010).

36. Shi, C., Roy, D., and Krivenko, P., "Alkali-Activated Cements and Concretes", ***CRC Press***, (2003).

37. Pacheco-Torgal, F., Castro-Gomes, J., and Jalali, S., "Alkali-activated binders: A review. Part 1. Historical background, terminology, reaction mechanisms and hydration products", ***Construction And Building Materials***, 22 (7): 1305–1314 (2008).

38. Palomo, A., Krivenko, P., Garcia-Lodeiro, I., Kavalerova, E., Maltseva, O., and Fernández-Jiménez, A., "A review on alkaline activation: new analytical perspectives", ***Materiales De Construcción***, 64 (315): e022 (2014).

39. Albidah, A., Alghannam, M., Abbas, H., Almusallam, T., and Al-Salloum, Y., "Characteristics of metakaolin-based geopolymer concrete for different mix design parameters", ***Journal Of Materials Research And Technology***, 10: 84–98 (2021).

40. Sundara Raman Chithiraputhiran, "Kinetics of Alkaline Activation of Slag and Fly ash-Slag Systems", ***Thesis***, (2012).

41. Edelhoff, D., & Özcan, M. (2007). To what extent does the longevity of fixed dental prostheses depend on the function of the cement? Working Group 4 materials: cementation. ***Clinical oral implants research***, 18, 193-204.

42. Van Deventer, J. S. J., Provis, J. L., Duxson, P., and Brice, D. G., "Chemical research and climate change as drivers in the commercial adoption of alkali activated materials", ***Waste And Biomass Valorization***, 1 (1): 145–155 (2010).

43. Provis, J. L. and Deventer, V., "Alkali-Activated Materials State-of-the-Art Report", (2014).

44. Van Jaarsveld, J. G. S., Van Deventer, J. S. J., and Lorenzen, L., "The potential use of geopolymeric materials to immobilise toxic metals: Part I. Theory and applications", ***Minerals Engineering***, 10 (7): 659–669 (1997).

45. Mo, B. H., Zhu, H., Cui, X. M., He, Y., & Gong, S. Y. (2014). Effect of curing temperature on geopolymerization of metakaolin-based geopolymers. Applied clay science, 99, 144-148.

46. Davidovits, J., "Geopolymer chemistry and sustainable development", (2005).

47. Duxson, P., Fernández-Jiménez, A., Provis, J. L., Lukey, G. C., Palomo, A., and van Deventer, J. S. J., "Geopolymer technology: the current state of the art", ***Journal Of Materials Science***, 42 (9): 2917–2933 (2007).

48. Fernández-Jiménez, A., Palomo, J. G., and Puertas, F., "Alkali-activated slag mortars", ***Cement And Concrete Research***, 29 (8): 1313–1321 (1999).

49. Palomo, Á., Alonso, S., Fernandez-Jiménez, A., Sobrados, I., and Sanz, J., "Alkaline Activation of Fly Ashes: NMR Study of the Reaction Products", ***Journal Of The American Ceramic Society***, 87 (6): 1141–1145 (2004).

50. Yip, C. K., Lukey, G. C., and van Deventer, J. S. J., "The coexistence of geopolymeric gel and calcium silicate hydrate at the early stage of alkaline activation", ***Cement And Concrete Research***, 35 (9): 1688–1697 (2005).

51. Law, D. W., Adam, A. A., Molyneaux, T. K., Patnaikuni, I., and Wardhono, A., "Long term durability properties of class F fly ash geopolymer concrete", ***Materials And Structures***, 48 (3): 721–731 (2015).

52. Fernández-Jiménez, A., Palomo, A., and Criado, M., "Microstructure development of alkali-activated fly ash cement: A descriptive model", ***Cement And Concrete Research***, 35 (6): 1204–1209 (2005).

53. Duxson, P. and Provis, J. L., "Designing Precursors for Geopolymer Cements", ***Journal Of The American Ceramic Society***, 91 (12): 3864–3869 (2008).

54. Wang, S.-D. and Scrivener, K. L., "29Si and 27Al NMR study of alkali-activated slag", ***Cement And Concrete Research***, 33 (5): 769–774 (2003).

55. Glukhovsky, V. ., "Alkaline cements and concretes", ***Proceedings Of The First International Conference Held At The Scientific-Research Institute On Binders And Materials Named After V.D. Glukhovsky***, 11–14 (1994).

56. Fernandez-Jimenez, A. and Puertas, F., "Setting of alkali-activated slag cement. Influence of activator nature", ***Advances In Cement Research***, 13 (3): 115–121 (2001).

57. Snyder, K. ., Feng, X., Keen, B. ., and Mason, T. ., "Estimating the electrical conductivity of cement paste pore solutions from OH−, K+ and Na+ concentrations", ***Cement And Concrete Research***, 33 (6): 793–798 (2003).

58. Ye, H., Huang, L., and Chen, Z., "Influence of activator composition on the chloride binding capacity of alkali-activated slag", ***Cement And Concrete Composites***, 104: 103368 (2019).

59. Shi, C. and Li, Y., "Effect of the modulus of water glass on the activation of phosphorus slag", ***Il Cemento***, 161–168 (1989).

60. Caijun, S. and Yinyu, L., "Investigation on some factors affecting the characteristics of alkali-phosphorus slag cement", ***Cement And Concrete Research***, 19 (4): 527–533 (1989).

61. Bondar, D., "Alkali Activation of Iranian Natural Pozzolans for Producing Geopolymer Cement and Concrete", ***Doctoral Thesis,The University Of Sheffield***, (June): (2009).

62. Nedeljković, M., "Carbonation Mechanism of Alkali-Activated Fly Ash and Slag Materials In View of Long-Term Performance Predictions", ***TU Delft University,*** 289 (2019).

63. Rai, S., Bahadure, S., Chaddha, M. J., and Agnihotri, A., "Disposal Practices and Utilization of Red Mud (Bauxite Residue): A Review in Indian Context and Abroad", ***Journal Of Sustainable Metallurgy***, 6 (1): 1–8 (2020).

64. Chandra, S., "Waste Materials Used in Concrete Manufacturing", (1996).

65. "World Aluminium — Alumina Production", .

66. Ribeiro, D. V., Labrincha, J. A., and Morelli, M. R., "Effect of the addition of red mud on the corrosion parameters of reinforced concrete", ***Cement And Concrete Research***, 42 (1): 124–133 (2012).

67. Reported by ACI Committee 232, "Use of Fly Ash in Concrete.", ***National Cooperative Highway Research Program, Synthesis Of Highway Practice***, 96 (Reapproved): 1–34 (1986).

68. "ASTM C618 - 03 Standard Specification for Coal Fly Ash and Raw or Calcined Natural Pozzolan for Use in Concrete", **https://www.astm.org/DATABASE.CART/HISTORICAL/C618-03.htm** (2021).

69. Pistorius, P. C., "Ilmenite smelting: The basics", ***Journal Of The Southern African Institute Of Mining And Metallurgy***, 108 (1): 35–43 (2008).

70 Al-Otaibi, S., "Durability of concrete incorporating GGBS activated by water-glass", ***Construction And Building Materials***, 22 (10): 2059–2067 (2008).

71. Chindaprasirt, P., Chareerat, T., and Sirivivatnanon, V., "Workability and strength of coarse high calcium fly ash geopolymer", ***Cement And Concrete Composites***, 29 (3): 224–229 (2007).

72. Flatt, R. J. **Towards a prediction of superplasticized concrete rheology**. Mat. Struct. 2004, 37, 289-300.

73. Roussel, N.; Lemaître, A.; Flatt, R. J.; Coussot, P. Steady state flow of cement suspensions: A micromechanical state of the art. C***ement and Concrete Research*** 2010, 40, 77-84.

74. Widjaja, B., & Lee, S. H. H. (2013). Flow box test for viscosity of soil in plastic and viscous liquid states**.** ***Soils and Foundations***, 53(1), 35-46.

75. Vyalov, S.S., 1986. Rheological Fundamentals of Soil Mechanics. Else- vier, Amsterdam, Netherlands.

76. Krizek, R.J. (2004): Slurries in Geotechnical Engineering. In: 12th Spencer J. ***Buchanan Lecture, Texas A&M University***, Texas, USA.

77. Mikhailov, N.M., Rebinder, P.A., 1955. On structural and mechanical properties of dispersed and high-olymeric systems. ***Colloid Journal*** 18, 2.

78. O'Brien, J.S., Julien, P.Y., 1988. Laboratory analysis of mudflow proper- ties. Journal of Hydraulic Engineering 114 (8), 877–887.

79. Ferraris, C., Winpigler, J., 2000. Bingham Model Concept-Measuring Rheological Properties of Cement-Based Materials. ***National Institute of Standard and Tech, Gaithersburg,*** USA.

80. Douglas, J.F., 1975. Solution of Problems in Fluid Mechanics. Pitman, London, UK.

81. Favier, A., Hot, J., Habert, G., de Lacaillerie, J. B. D. E., & Roussel, N. (2013, September). Rheology of geopolymer: comparative study between Portland cement and metakaolin based geopolymer**.** ***In 1st RILEM International Conference on Rheology and Processing of Construction Materials***., RILEM Publications sarl, Paris: France (pp. 49-56).

82. Lal, R., Shukla, M.K., 2004. Principles of Soil Physics**.** Marcel Dekker, New York, USA.

83. Dinger, D.R., 2002. Rheology for Ceramists. ***Morris Publishing, Kearney***, USA.

84. Metzner AB, Reed JC. Flow of non-Newtonian fluids—correlation of the laminar, transition, and turbulent-flow regions. AICHE J. 1955;1(4):434-440.

85. Bingham EC. An investigation of the laws of plastic flow. Bull Bureau Stand. 1917;13(278):309-353. ***Washington: US Government Printing Office.***

86. Wallick GC, Savins JG. A comparison of differential and integral descriptions of the annular flow of a power-law fluid**.** SPE J. 1969;9(03):311-315.

87. Casson N. A flow equation for pigment-oil suspensions of the printing ink type. Rheology of Disperse Systems. (pp. 84-104). New York, NY: Pergamon Press; 1959.

88. Herschel WH, Bulkley R. Measurement of consistency as applied to rubber-benzene solutions**.** Am Soc Test Proc. 1926;26(2):621-633.

89. Andaverde JA, Wong-Loya JA, Vargas-Tabares Y. A practical method for determining the rheology of drilling fluid**.** J **Petrol Sci Eng**. 2019;180:150-158.

90. ASTM 2009 DE6910/D6910M: Standard Test method for Marsh funnel Viscosity of Clay Construction slurries.

91. Bingham, E.C., 1922. Fluidity and plasticity. McGraw-Hill.

92. Balhoff, M.T.; Lake, L.W., Bommer, P.M.; Lewis, R.E.; Weber, M.J.; Calderin, J.M., 2011. Rheological and yield stress measurement of non-Newtonian fluids using a Marsh-funnel**.** ***Journal of petroleum Science and Engineering,*** Vol. 77, pp. 393-402.

93. H. Marsh, Properties and Treatment of Rotary Mud. Petroleum Development and Technology, Transactions of the AIME (1931), pp. 234–251.

94. Almahdawi, F. H., Al-Yaseri, A. Z., & Jasim, N. (2014). **A**pparent viscosity direct from Marsh funnel test. **Iraqi Journal of Chemical and Petroleum Engineerin**g, 15(1), 51-57.

95. M.J. Pitt,The Marsh Funnel and drilling fluid **viscosity**: a new equation for field use. Soc. ***Petroleum Eng., Drilling Completions***, 15 (1) (2000), pp.3–6.

96. Widayanti, A., Soemitro, R. A. A., Suprayitno, H., & Ekaputri, J. J. (2018). Characterization and compressive strength of fly ash based-geopolymer paste**.** I***n MATEC Web of Conferences (***Vol. 195, p. 01023). EDP Sciences.

97. Lv, Q., Yu, J., Ji, F., Gu, L., Chen, Y., & Shan, X. (2021). Mechanical Property and Microstructure of Fly Ash-Based Geopolymer Activated by Sodium Silicate. ***KSCE Journal of Civil Engineering***, 25(5), 1765-1777.

98. Saha, S., & Rajasekaran, C. (2017). Enhancement of the properties of fly ash based geopolymer paste by incorporating ground granulated blast furnace slag. ***Construction and Building Materials,*** 146, 615-620.

99. Madai, F., Kristaly, F., & Mucsi, G. (2015). Microstructure, mineralogy and physical properties of ground fly ash based geopolymers**.** Ceramics–Silikáty, 59(1), 70-79.

100. Nergis, D. D. B., Abdullah, M. M. A. B., & Vizureanu, P. (2017). The effect of fly ash/alkaline activator ratio in class f fly ash based geopolymers. ***Euro J Mater Sci Eng,*** 2(4), 111-118.

101. Oderji, S. Y., Chen, B., Ahmad, M. R., & Shah, S. F. A. (2019). Fresh and hardened properties of one-part fly ash-based geopolymer binders cured at room temperature: Effect of slag and alkali activators. ***Journal of Cleaner Production,*** 225, 1-10.

102. Chattopadhyay, S., Mondal, S., Barman, B., Ghosh, K., & Ghosh, P. effect of addition of chemical admixture on the physico-mechanical and microstructural properties of a fly ash-slag blended geopolymer composite.

103. Raju, T., Ramaswamy, K. P., & Saraswathy, B. (2020, June). Effects of slag and superplasticizers on alkali activated geopolymer paste. ***In IOP Conference Series***: Earth and Environmental Science (Vol. 491, No. 1, p. 012042). IOP Publishing.

104. Nematollahi, B., & Sanjayan, J. (2014). Effect of different superplasticizers and activator combinations on workability and strength of fly ash based geopolymer. ***Materials & Design***, 57, 667-672.

105 Samantasinghar, S., & Singh, S. P. (2019). Fresh and hardened properties of fly ash–slag blended geopolymer paste and mortar. ***International Journal of Concrete Structures and Materials,*** 13(1), 1-12.

106. Mallikarjuna Rao, G., & Gunneswara Rao, T. D. (2015). Final setting time and compressive strength of fly ash and GGBS-based geopolymer paste and mortar. ***Arabian Journal for Science and Engineering***, 40(11), 3067-3074.

107. Pothinathan, S. K. M., Millar, J., & Gnanaraj, S. C. (2021)**.** Effect of Sulfonated-Melamine Formaldehyde as Superplasticizer in Cementitious Systems. ***Recent Advancements in Geotechnical Engineering:*** NCRAG'21, 19, 51.

108. Laskar, M. S., & Talukdar, S. (2018). Influence of superplasticizer and alkali activator concentration on slag–fly ash based geopolymer. Urbanization Challenges in Emerging Economies, 330-337.

109. Nuruddin, M. F., Demie, S., Ahmed, M. F., & Shafiq, N. (2011). Effect of superplasticizer and NaOH molarity on workability, compressive strength and microstructure properties of self-compacting geopolymer concrete. ***International Journal of Geological and Environmental Engineering,*** 5(3), 187-194.

110. Razak, S., Zainal, F. F., & Shamsudin, S. R. (2020, October). Effect of porosity and water absorption on compressive strength of fly ash based geopolymer and OPC Paste. ***In IOP Conference Series***: Materials Science and Engineering (Vol. 957, No. 1, p. 012035). IOP Publishing.

111. Ahmad Zailani, W. W., Bouaissi, A., Abdullah, M. M. A. B., Abd Razak, R., Yoriya, S., Mohd Salleh, M. A. A. & Fansuri, H. (2020). Bonding strength characteristics of FA-based geopolymer paste as a repair material when applied on opc substrate. ***Applied Sciences***, 10(9), 3321.

112. Puertas, F., Varga, C., & Alonso, M. M. (2014). Rheology of alkali-activated slag pastes. Effect of the nature and concentration of the activating solution. ***Cement and Concrete Composites,*** *53*, 279-288.

113. Schwieger, W., & Lagaly, G. (2004). Alkali silicates and crystalline silicic acids. ***Handbook of Layered Materials***, 541-630.

114. Berkovitch, I., "Admixtures for Concrete.", ***Civil Engineering London***, 29–31 (1984).

115. Shanahan, N. G., "Interaction of Cementitious Systems with Chemical Admixtures", 180 (2016).

116. ASTM C348, A., "Flexural strength of hydraulic-cement mortars", ***American Society for Testing and Material***, (2018).

117. Schwieger, W., & Lagaly, G. (2004). Alkali silicates and crystalline silicic acids. ***Handbook of Layered Materials***, 541-630.

118. Mittal, M., & Chaudhary, R. (2018). Experimental investigation on the mechanical properties and water absorption behavior of randomly oriented short pineapple/coir fiber-reinforced hybrid epoxy composites. ***Materials Research Express***, *6*(1), 015313.

119. Patankar, S. V., Ghugal, Y. M., & Jamkar, S. S. (2014). Effect of concentration of sodium hydroxide and degree of heat curing on fly ash-based geopolymer mortar. ***Indian Journal of Materials Science***, 2014.

## RESUME

Noora Khasro SALEH after she had completed her high school education at high school in Kirkuk/Iraq (Kirkuk High School for the Distinguished), she taken a bachelor's degree from Kirkuk/in Civil Engineering in 2015. To complete their M.Sc., he moved to Karabuk/Turkey in 2020. She started his master's education at the department of civil engineering at Karabuk University and taken graduate degree from the same department in 2022.